Doping dependence of spin excitations in the stripe phase of high-T_c superconductors

G. Seibold
Institut für Physik, BTU Cottbus, P.O. Box 101344, 03013 Cottbus, Germany

J. Lorenzana
SMC-INFM, ISC-CNR, Dipartimento di Fisica, Università di Roma La Sapienza, P. Aldo Moro 2, 00185 Roma, Italy
(Received 14 September 2005; revised manuscript received 23 January 2006; published 25 April 2006)

Based on the time-dependent Gutzwiller approximation for the extended Hubbard model, we calculate the energy and momentum dependence of spin excitations for striped ground states. Our starting point correctly reproduces the observed doping dependence of the incommensurability in La-based cuprates and the dispersion of magnetic modes in the insulating parent compound. This allows us to make quantitative predictions for the doping evolution of the dispersion of magnetic modes in the stripe phase including the energy ω_0 and intensity of the resonance peak as well as the velocity c of the spin-wave-like Goldstone mode. In the underdoped regime $n_h<1/8$, we find a weak linear dependence of ω_0 on doping, whereas the resonance energy significantly shifts to higher values when the charge concentration in the stripes starts to deviate from half-filling for $n_h>1/8$. The velocity c is nonmonotonous with a minimum at $1/8$ in coincidence with a well known anomaly in T_c. Our calculations are in good agreement with available experimental data. We also compare our results with analogous computations based on linear spin-wave theory.

DOI: 10.1103/PhysRevB.73.144515 PACS number(s): 74.72.−h, 71.10.−w, 71.28.+d, 74.25.Ha

I. INTRODUCTION

The development of a theory for high-T_c superconductivity presupposes a detailed understanding of the normal state collective excitations in the charge and magnetic channels. This paper is devoted to the latter channel where we explore the spectrum of spin fluctuations based on a stripe scenario extending the results presented in a previous short communication.[1]

The large variety of cuprate materials has often narrowed the view on the properties of individual compounds rather than the common features between them. In $YBa_2Cu_3O_y$ (YBCO) compounds, inelastic neutron scattering (INS) experiments have usually emphasized the "resonance mode,"[2–6] an inelastic feature that sharpens as a δ-like excitation at frequency ω_0 below T_c and is located around the commensurate antiferromagnetic (AF) wave vector $\mathbf{Q}_{\mathrm{AF}}=(\pi,\pi)$ (we set the lattice constant $a\equiv 1$ and restore it when convenient for clarity). On the other hand, in lanthanum-based cuprates (LCO) the emphasis has been put on incommensurate features, either elastic or low-energy inelastic as, for example, Goldstone-like modes emerging from incommensurate wave vectors.[7–13]

In LCO, the incommensurate low-energy magnetic scattering occurs at wave vectors $\mathbf{Q}_s=(\pi\pm 2\pi\epsilon,\pi)$ and $(\pi,\pi\pm 2\pi\epsilon)$ and ϵ depends linearly on doping $\epsilon=n_h$ up to $n_h\approx 1/8$.[10] Here n_h is the number of added holes per planar Cu with respect to the parent insulating compound. This behavior is compatible with stripelike modulations of charge and spin having a linear concentration of added holes $\nu=1/2$ (so-called half-filled stripes), that is $\sim$ 1 hole per every second elementary unit cell along the stripe and with charge (spin) periodicity d $(2d)$ perpendicular to the stripe so that $\epsilon=1/(2d)$ and $n_h=\nu/d$.

Regarding superconductivity, Wakimoto and collaborators[14] have recently found a direct relation between T_c and the intensity of low-energy scattering in the overdoped regime that together with other studies[15] establishes a direct relation between superconductivity and incommensurate scattering parallel to the Cu-O bond across the full phase diagram of LCO compounds and makes more stringent the understanding of the magnetic excitations.

Despite the different emphasis mentioned above, some investigations in recent years have started to focus on common features suggesting a universal phenomenology in the spin dynamics between different classes of high-T_c cuprates. These similarities comprise the low-energy incommensurate scattering in YBCO,[16] which has a similar dependence on doping as in LCO, namely a linear increase at small doping followed by a saturation at larger concentrations. Even static incommensurate order has been reported[17] in strongly underdoped YBCO. Moreover, in detwinned samples of YBCO, the incommensurate scattering has been shown to be anisotropic suggesting underlying stripe correlations.[18] The presence of a "rigid stripe array" has been questioned in the more recent Ref. 19, which also reports an anisotropic response although in a more subtle way. We will come back to this point in Sec. IV.

Finally, recent INS measurements show a remarkable similarity of the magnetic response of $La_{2-x}Ba_xCuO_4$ (LBCO) (Ref. 11) and YBCO (Ref. 20) over a broad range of momenta and energy. Both experiments have revealed low-energy incommensurate excitations which, with increasing energy, continuously disperse toward the resonance mode at $\mathbf{Q}_{\mathrm{AF}}$.[11,20] An INS study on optimally doped $La_{2-x}Sr_xCuO_4$ (LSCO) (Ref. 13) has also resolved the dispersion of the spin-wave modes emerging from the incommensurate positions which closely resemble corresponding data of $YBa_2Cu_3O_{6.85}$.[21]

Above ω_0, the magnetic excitations start to form a ring- or square-shaped pattern around $\mathbf{Q}_{\mathrm{AF}}$ which increases in size with increasing energy. In twinned samples, low-energy

acoustic modes together with the high-energy excitations thus display an "X"-like dispersion. These features are now well established in both LCO (eventually codoped with Nd or Ba) (Refs. 11 and 13) and YBCO (Refs. 6, 19, 20, and 22–24) while in Bi (Ref. 25) and Tl materials[26] only the resonance peak has been resolved.

The two most prominent explanations for the features in the magnetic scattering are (a) a scenario based on dispersing particle-hole bound states induced by the antiferromagnetic (AFM) correlations in a d-wave superconducting system[27–35] and (b) theories that rely on the presence of stripe correlations in the ground state of the system.[1,36–42] Approaches belonging to (a) are rather popular in describing spin excitations in the superconducting state of YBCO materials. The ground state is assumed to be a homogeneous metal from the start.[27–34] Superconductivity on top of this induces a spin gap on the dynamical susceptibility and a random-phase approximation (RPA) resummation of the AFM interaction creates exciton peaks in the imaginary part of the magnetic susceptibility. Due to the special frequency and momentum structure of the noninteracting spin response functions in a d-wave superconducting system, the strongest weight is acquired by the "resonance peak" at the AFM wave vector and frequency ω_0 close to the spin-gap energy. Above and below ω_0 also an incommensurate response can be obtained, the structure of which strongly depends on the underlying tight-binding dispersion. This "excitonic" picture finds support in the fact that in optimally doped YBCO the resonance appears below T_c and offers a natural explanation for the relation $\omega_0 \sim kT_c$ as observed in YBCO (see, e.g., Ref. 5). However, in underdoped YBCO the resonance is observed above T_c,[4] and upon applying this approach to a quantitative description of magnetic excitations in LSCO, it has been shown to be incompatible with the low-energy response.[31,32] Moreover, in order to properly account for the doping dependence of the low-energy incommensurability in YBCO, this approach has to rely on peculiar nesting properties of the Fermi surface over a large doping range.[43]

The incommensurate correlations observed on several compounds have encouraged theories based on the presence of stripe correlations in the ground state of the system.[1,36,37,39–42,44,45] The starting point is a broken symmetry state where at least C_4 lattice symmetry is broken, translation symmetry is usually broken (at least in explicit computations), and the breaking of SU(2) spin rotational symmetry depends on the approach. If SU(2) is conserved as in Refs. 36, 37, and 39, the system has a spin gap in the spectrum, whereas if it is broken,[1,40–42,44,45] as in the present work, one finds a Goldstone magnetic mode emerging from the incommensurate wave vector. A spin gap is observed in YBCO compounds, whereas a Goldstone-like mode is observed in LCO. The response of both systems is very similar above the gap.[13] We will come back to this point in Sec. V.

In our SU(2) broken approach, at small doping, partially filled stripes are stable[46,47] explaining the linear dependence of the incommensurability on doping for $n_h < 1/8$.[48–51] Our previous computations in the Gutzwiller approximation (GA)[50,51] have shown that due to their transverse extension, stripes with $d < 4$ are energetically unfavorable so that for $n_h > 1/8$ the incommensurability remains at $\epsilon \approx 1/8$ in accord with experiment and the stripe filling starts to increase beyond the value $\nu = 1/2$. This picture is also in agreement with dynamical mean-field theory computations.[48,49]

Within this scenario, the resonance feature appears as a saddle point (or a local maximum) in the dispersion relation of magnetic excitations as quantitatively evaluated for LBCO in our previous work.[1] The idea that the resonance may be seen as the lowest energy magnetic excitation at $\mathbf{Q}_{\mathrm{AF}}$ in an incommensurate system was already proposed in Ref. 52.

Within the stripe scenario, another line of thought has appeared based on simplified effective spin-only models. These studies map the stripe structure to an array of coupled n-leg spin ladders with n even. This makes it possible to consider states where SU(2) is not broken and which exhibit a spin gap as in YBCO.[36–39] However, for some dopings n is expected to be odd and the system should be gapless. We are not aware of evidence for this even/odd phenomenon.

In this paper, we present detailed computations of the dynamical magnetic structure factor on top of the static GA stripe textures using the time-dependent Gutzwiller approximation (TDGA).[53,54] In addition, we compare the TDGA results with linear spin-wave theory (LSWT) computations. We present the doping dependence of magnetic excitations extending our previous results[1] for doping $n_h = 1/8$. To be specific, we choose parameters as appropriate for LBCO or LSCO where our investigation provides a quantitative prediction for the relation between ω_0, the spin-wave velocity, the dispersion of high-energy modes, etc. as a function of doping n_h. As in our previous report,[1] parameters are fixed by fitting the dispersion relation in the insulator and by requiring the correct filling ν of the stripes. For the rest, the computations in the doped phase can be considered without free parameters and are in good agreement with data at $n_h = 1/8$ (Ref. 11) on LBCO. We compare the new results with experimental data[13] at $n_h = 0.1$ and 0.16. Encouraged by the experimental finding of universality of spin excitations in different cuprate materials, we also attempt to make a connection of our results with experimental features observed in YBCO materials. In this case, however, due to the presence of the spin gap and the bilayer structure, our results will be more qualitative than quantitative.

This paper is organized as follows. In Sec. II, we present the model and outline the formalism for the computation of magnetic excitations. In Sec. III, we show how the appropriate parameter set can be obtained from experimental and theoretical considerations. In addition, we present the saddle-point solutions on which the subsequent RPA fluctuations are computed. In Sec. IV, we present results for the doping dependence of magnetic excitations in the stripe phase and discuss these spectra with respect to the present experimental situation. Finally, we conclude our considerations in Sec. V.

II. MODEL AND FORMALISM

Our investigations are based on the one-band Hubbard model with hopping restricted to nearest ($t_{ij} = -t$) and next nearest ($t_{ij} = -t'$) neighbors

$$H = \sum_{ij,\sigma} t_{ij} c^{\dagger}_{i,\sigma} c_{j,\sigma} + U \sum_{i} n_{i,\uparrow} n_{i,\downarrow}. \tag{1}$$

Here $c^{(\dagger)}_{i,\sigma}$ destroys (creates) an electron with spin σ at site i, and $n_{i,\sigma} = c^{\dagger}_{i,\sigma} c_{i,\sigma}$. U is the on-site Hubbard repulsion.

A. Time-dependent Gutzwiller approximation

As a starting point we treat the model Eq. (1) within an unrestricted Gutzwiller approximation (GA) in the spin-rotational invariant formulation.[55–57] Basically one constructs a Gutzwiller wave function $|\Psi\rangle$ by applying a projector to a Slater determinant $|\mathrm{SD}\rangle$ which reduces the double occupancy. The Slater determinant is allowed to have an inhomogeneous charge and spin distribution describing generalized spin and charge density waves determined variationally.[58]

The resulting energy functional $E^{\mathrm{GA}} \equiv \langle \Psi | H | \Psi \rangle$ treated in the Gutzwiller approximation reads as[54]

$$E^{\mathrm{GA}} = \sum_{i,j,\sigma,\sigma_1,\sigma_2} t_{ij} z_{i,\sigma_1,\sigma} z_{j,\sigma,\sigma_2} \langle c^{\dagger}_{i\sigma_1} c_{j\sigma_2} \rangle_0 + U \sum_i D_i, \quad (2)$$

where the matrix $\mathbf{z}_i$ is given by

$$\mathbf{z}_i = \begin{pmatrix} z_i^+ \cos^2 \frac{\Phi}{2} + z_i^- \sin^2 \frac{\Phi}{2} & \frac{S_i^-}{S_i^z}[z_i^+ - z_i^-]\cos\Phi \\ \frac{S_i^+}{S_i^z}[z_i^+ - z_i^-]\cos\Phi & z_i^+ \sin^2 \frac{\Phi}{2} + z_i^- \cos^2 \frac{\Phi}{2} \end{pmatrix} \quad (3)$$

and

$$\tan^2 \Phi = \frac{S_i^+ S_i^-}{(S_i^z)^2},$$

$$z_i^{\pm} = \frac{\sqrt{1 - n_i + D_i}\lambda_i^{\pm} + \lambda_i^{\mp}\sqrt{D_i}}{\sqrt{[1 - D_i - (\lambda_i^{\pm})^2][n_i - D_i - (\lambda_i^{\mp})^2]}},$$

$$(\lambda_i^{\pm})^2 = n_i/2 - D_i \pm S_i^z \sqrt{1 + \tan^2 \Phi}.$$

The above expressions are given in terms of the one-body density matrix $\rho_{i\sigma,j\sigma'} \equiv \langle c^{\dagger}_{i\sigma} c_{j\sigma'} \rangle_0$ in the Slater determinant $|\mathrm{SD}\rangle$. For brevity, we denote such averages with $\langle \cdots \rangle_0$ and introduce the notations $S_i^+ \equiv \langle c^{\dagger}_{i\uparrow} c_{i\downarrow} \rangle_0$, $n_i \equiv \Sigma_\sigma \langle c^{\dagger}_{i\sigma} c_{i\sigma} \rangle_0$, etc.

In order to obtain generally inhomogeneous solutions (stripes, etc.), one has to minimize Eq. (2) with respect to the double occupancy parameters $D_i = \langle \Psi | n_{i\uparrow} n_{i\downarrow} | \Psi \rangle$ and with respect to ρ under the constraint that ρ corresponds to a Slater determinant. For simplicity, we restrict our saddle-point solutions to the limit $S_i^{\pm} = 0$, where the matrix $\mathbf{z}_i$ is diagonal and the standard Gutzwiller energy functional as derived by Gebhard[58] or Kotliar and Ruckenstein is recovered.[59] (The spin-rotational invariant formulation is necessary for the fluctuation computation.)

We have previously shown that with realistic parameters this approach leads to vertical, metallic stripes in agreement with experimental data.[50,51] Here we have repeated these calculations in large systems typically consisting of $N \sim 100 \times 100$ lattice sites in order to obtain sufficient momentum resolution for the computation of spin excitations. For stripes oriented along the y direction this is most conveniently done by decomposing the lattice into N_{cells} unit cells of size $N_a = d \times 2$ with $N = N_{\mathrm{cells}} N_a$. The unit cell for the $d=4$ solution is schematized in Fig. 1. The locations of the unit cells define a Bravais "superlattice."[60] The positions of the Bravais superlattice are given by $\mathbf{R} \equiv n_1 \mathbf{a}_1 + n_2 \mathbf{a}_2$ with n_i integer. For even d the Bravais lattice is generated by the elementary translations $\mathbf{a}_1 = (d, 1)$ and $\mathbf{a}_2 = (0, 2)$, whereas for d being odd we have $\mathbf{a}_1 = (d, 0)$ and $\mathbf{a}_2 = (0, 2)$. From the translation vectors we can obtain the generators $\mathbf{b}_i$ of the reciprocal superlattice defined by the relation $\mathbf{a}_i \cdot \mathbf{b}_j = 2\pi\delta_{ij}$ and construct the associated magnetic Brillouin zone (MBZ). For odd d the latter is simply a rectangle spanned by the reciprocal superlattice vectors $\mathbf{b}_1 = (2\pi/d, 0)$ and $\mathbf{b}_2 = (0, \pi)$, whereas for even d the shape is more complex due to the nonorthogonality of the translation vectors.

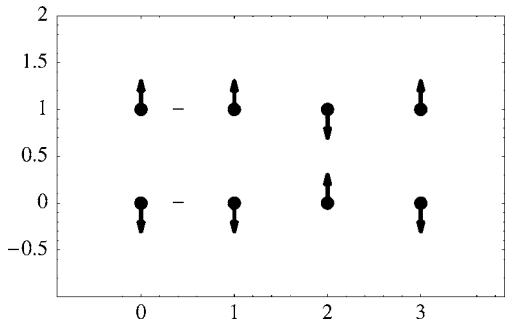

FIG. 1. Unit cell used for the $d=4$ stripe computation. The length of the spin arrows corresponds to the LSWT computations. (For the GA computations, the spin magnitude is modulated as shown in Fig. 4.) We also show the interactions used in the LSWT computation: a uniform value of the AFM interaction J across all the bonds except for the ferromagnetic bonds where the sign is opposite to ensure stability and the modulus is $J_F = 0.2J$.

As an example we show in Fig. 2 the first magnetic Brillouin zone (MBZ) and the extended Brillouin zone (EBZ) for

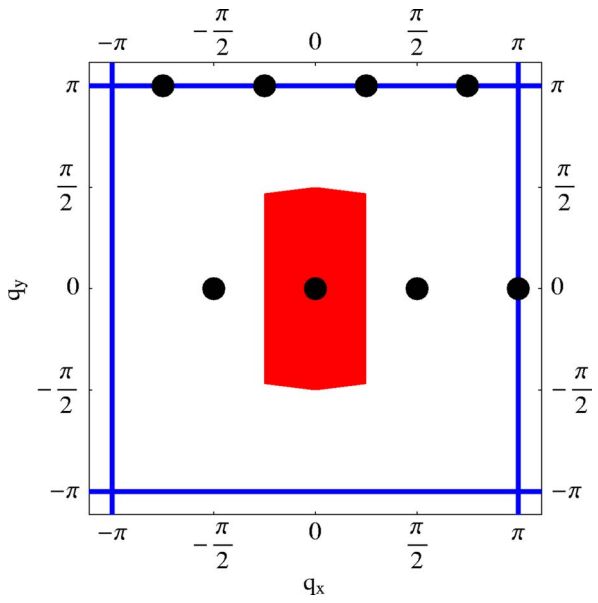

FIG. 2. (Color online) The central polygon is the first magnetic Brillouin zone for $d=4$ stripes. Thick lines enclose the extended Brillouin zone. The dots are a set of magnetic reciprocal superlattice vectors that define a set of higher magnetic Brillouin zones with total volume equal to the EBZ volume. Magnetic modes and single-particle states can be classified by the momentum in the central magnetic Brillouin zone and a band index. The magnetic reciprocal superlattice vectors closest to $(\pm\pi, \pm\pi)$ are referred to as Q^s.

$d=4$ stripes. The momenta in the EBZ label the N plane-wave states of the system. Alternatively one can label the plane-wave states by a reduced momentum $\tilde{\mathbf{k}}$ in the first MBZ (the central polygon in Fig. 2) and a set of N_a reciprocal superlattice vectors $\mathbf{Q}\equiv m_1\mathbf{b}_1+m_2\mathbf{b}_2$ with m_i integer, the momentum of the plane-wave state being given by $\mathbf{Q}+\tilde{\mathbf{k}}$. The dots in Fig. 2 indicate a possible choice for this set. Each dot defines also a higher MBZ with the dot at the center.

Magnetic excitations are obtained by computing random-phase approximation (RPA)-like fluctuations on top of the GA saddle point[53,54] within the TDGA which fulfills standard sum rules and on small clusters yields excitation spectra in very good agreement with exact diagonalization.[54]

The basic ingredient of this approach is the interaction kernel. In the spin channel this is obtained by expanding Eq. (2) up to second order in the spin fluctuations,[54]

$$\delta E^{\text{spin}} = \sum_{ij} V_{ij}\delta S_i^+\delta S_j^- + \sum_{ij} M_{ij}^{\uparrow}[\delta S_i^+\delta\langle c_{i\downarrow}^\dagger c_{j\uparrow}\rangle_0 + \delta\langle c_{j\uparrow}^\dagger c_{i\downarrow}\rangle_0\delta S_i^-] + \sum_{ij} M_{ij}^{\downarrow}[\delta S_i^+\delta\langle c_{j\downarrow}^\dagger c_{i\uparrow}\rangle_0 + \delta\langle c_{i\uparrow}^\dagger c_{j\downarrow}\rangle_0\delta S_i^-]. \tag{4}$$

Here we have defined the following interaction matrices:

$$V_{ii} = \sum_{j,\sigma} t_{ij}[\langle c_{i\sigma}^\dagger c_{j\sigma}\rangle_0 + \langle c_{j\sigma}^\dagger c_{i\sigma}\rangle_0]z_{j,\sigma,\sigma}^0\frac{\partial^2 z_{i,\sigma,\sigma}}{\partial S_i^+\,\partial\, S_i^-}, \tag{5}$$

$$V_{i\neq j} = t_{ij}[\langle c_{i\uparrow}^\dagger c_{j\uparrow}\rangle_0 + \langle c_{j\downarrow}^\dagger c_{i\downarrow}\rangle_0]\frac{\partial z_{i,\uparrow,\downarrow}}{\partial S_i^+}\frac{\partial z_{i,\downarrow,\uparrow}}{\partial S_i^-}, \tag{6}$$

$$M_{ij}^{\sigma} = t_{ij}z_{j,\sigma,\sigma}^0\frac{\partial z_{i,\uparrow,\downarrow}}{\partial S_i^+}. \tag{7}$$

Basically the TDGA is closely related to the time-dependent Hartree-Fock (HF) approximation which in the limit of small oscillations corresponds to the RPA.[63] The structure of the equations is the same but the interaction kernel is substantially different. Indeed, in the present approach there is a space dependency of the effective on-site term V_{ii} (instead of the bare "U") which follows the modulation of the underlying saddle-point solution (cf. Fig. 4). In addition, the GA+RPA formalism generates effective interactions between spin fluctuations on different sites ($\sim V_{i\neq j}$) and between intersite spin-flip processes ($\sim M_{ij}^{\sigma}$). However, the strength of the latter interactions is in general much smaller than the on-site contribution V_{ii}.

In order to evaluate the RPA series, we first have to evaluate the ("zeroth order") susceptibilities on the GA level, e.g.,

$$\chi_{nm}^{st,0}(\tilde{\mathbf{q}},\omega) = \frac{i}{N}\int dt e^{-i\omega t}\langle\mathcal{T}A^s(\tilde{\mathbf{q}}+\mathbf{Q}_n,t)A^t(-\tilde{\mathbf{q}}-\mathbf{Q}_m,0)\rangle_{\text{GA}}. \tag{8}$$

Here the vector $\{A^s\}$ is composed of the following operators: $A_n^1\equiv\hat{S}^+(\tilde{\mathbf{q}}+\mathbf{Q}_n)$ is the momentum representation of the local spin fluctuation $S_i^+=c_{i\uparrow}^\dagger c_{i\downarrow}$. $A_n^{1+\alpha}\equiv T^\alpha(\tilde{\mathbf{q}}+\mathbf{Q}_n)$ are the Fourier transformed operators of the intersite spin fluctuations $c_{i\uparrow}^\dagger c_{i+R\alpha\downarrow}$. Both fluctuations are mixed by the term M_{ij}^{σ} in Eq. (4) (cf. Ref. 54 for details). For a model with next- and next-nearest-neighbor hopping, we have $\alpha=1,\ldots,8$ orthogonal operators $T^\alpha(\tilde{\mathbf{q}}+\mathbf{Q}_n)$ so that together with $S^+(\tilde{\mathbf{q}}+\mathbf{Q}_n)$ the complete zeroth-order correlation function $\chi_{nm}^{st,0}(\tilde{\mathbf{q}},\omega)$ is an $18d\times 18d$ matrix. On the other hand, we can also express the Fourier transformed interaction Eq. (4) in terms of an $18d\times 18d$ dimensional matrix $\underline{\underline{\Gamma}}(\tilde{\mathbf{q}})$

$$\delta E^{\text{spin}} = \sum_{stmn} A^s(\tilde{\mathbf{q}}+\mathbf{Q}_n)\Gamma_{nm}^{st}(\tilde{\mathbf{q}})A^t(-\tilde{\mathbf{q}}-\mathbf{Q}_m) \tag{9}$$

so that formally the RPA summation can be written as

$$\underline{\underline{\chi}}(\tilde{\mathbf{q}}) = \underline{\underline{\chi}}^0(\tilde{\mathbf{q}}) - \underline{\underline{\chi}}^0(\tilde{\mathbf{q}})\underline{\underline{\Gamma}}(\tilde{\mathbf{q}})\underline{\underline{\chi}}(\tilde{\mathbf{q}}). \tag{10}$$

Upon inverting this equation, we finally obtain the transverse spin correlation function as $\chi_{nm}^{\perp}(\tilde{\mathbf{q}})\equiv\chi_{nm}^{11}(\tilde{\mathbf{q}})$.

B. Spin-wave theory calculations

In order to interpret the GA+RPA results, we have made a LSWT computation of the dispersion similar to those performed in Refs. 41 and 42. For simplicity we take a model with only AFM nearest-neighbor magnetic interactions J equal everywhere except for the ferromagnetic bonds where the interaction has opposite sign (to ensure stability) and magnitude J_F as shown schematically in Fig. 1.

C. Dynamical structure factor

Neutron scattering experiments probe the longitudinal and transverse components of the dynamical structure factor $S^{\alpha\beta}(\boldsymbol{q},\omega)$ weighted by polarization factors,[66,67]

$$S^{\text{eff}}(\boldsymbol{q},\omega) = \sum_\alpha\langle(1-\hat{q}_\alpha^2)\rangle_{\text{dom}}S^{\alpha\alpha}(\boldsymbol{q},\omega) = \eta_\parallel S^\parallel(\boldsymbol{q},\omega) + \eta_\perp S^\perp(\boldsymbol{q},\omega), \tag{11}$$

where $\boldsymbol{q}\equiv\boldsymbol{k}-\boldsymbol{k}'$ ($\hat{\boldsymbol{q}}\equiv\mathbf{q}/|\boldsymbol{q}|$), $\boldsymbol{k}$ ($\boldsymbol{k}'$) is the initial (final) wave vector of neutrons, and an average over the orientation of domains, $\langle\cdots\rangle_{\text{dom}}$, has been done. In Eq. (11), we have defined the longitudinal ($\parallel$) and transverse contributions ($\perp$) with respect to the ordered magnetic moment.

Unpolarized experiments are sensitive to relatively sharp features which are expected to correspond mainly to transverse fluctuations,[67] therefore in the present study we restrict to the latter $S^{\text{eff}}\approx\eta_\perp S^\perp$. The average polarization factor $\eta_\perp$ depends on the orientation of the magnetic domains. For a distribution of domains isotropic in spin space, $\eta_\perp=2/3$. For a nonisotropic distribution, $\eta_\perp$ depends also on the scattering geometry with the minimum value $\eta_\perp=1/2$.[67]

In terms of the reduced momentum $\tilde{\mathbf{q}}$ and the reciprocal superlattice vector $\mathbf{Q}_n$ defined in the previous subsection, the structure factor is given by

$$S^\perp(\tilde{\mathbf{q}}+\mathbf{Q}_n,\omega) = \frac{(g\mu_B)^2}{\pi}Z_d\int dt\,\exp(-i\omega t)\text{Im}\chi_{nn}^\perp(\tilde{\mathbf{q}},t). \tag{12}$$

Here we have included an intensity renormalization Z_d similar to LSWT. For a half-filled system with a SDW and in the

limit of large U, GA+RPA, HF+RPA, and LSWT give the same results. The latter is well known to overestimate the intensities of the spin-wave modes roughly by a factor of 2 and the same problem arises in the RPA approaches. GA +RPA, HF+RPA interpolate smoothly between this strong-coupling limit and the noninteracting case, however in the latter case $Z_d=1$. The value appropriate for cuprate parameters will be intermediate between these two limits. We refer to Ref. 67, where Z_d and $\eta_\perp$ are discussed in detail.

$S^\perp(\mathbf{q},\omega)$ in general acquires different weight in MBZ's centered on different $\mathbf{Q}_n$ (cf. Fig. 2). Since we are not considering the magnetic form factor, $S^\perp(\mathbf{q},\omega)$ repeats with the periodicity of the EBZ reciprocal-lattice vectors $(0,2\pi)$ and $(2\pi,0)$.

The stripes correspond to a long-range magnetically ordered state which within our RPA-like scheme induces a Goldstone mode going to zero frequency at momenta $\tilde{\mathbf{q}}=\mathbf{0}$. However, this mode has negligible weight at $\mathbf{q}\sim\mathbf{0}$ but acquires a significant strength in the higher magnetic zones at $\tilde{\mathbf{q}}+\mathbf{Q}$ with the magnetic reciprocal-lattice vector $\mathbf{Q}\neq\mathbf{0}$. The largest spectral weight, as shown below, is located at the dots closest to $(\pm\pi,\pm\pi)$ in Fig. 2. These points are referred to as the incommensurate wave vector $\mathbf{Q}_s$.

III. PARAMETERS AND SADDLE-POINT SOLUTIONS

With respect to our previous investigation,[1] we have significantly improved the resolution in frequency and momentum space which allows us to consider up to 10 000 lattice sites and frequency intervals of $\sim$1 meV as discussed in the preceding section. Within the present one-band description, we fix parameters by the following two conditions.

(i) The value of the nearest-neighbor hopping has been fixed to $t'/t=-0.2$ according to Refs. 51 and 68. In Ref. 51, we found that the stripe filling is very sensitive to t'/t and it turned out that a ratio of $t'/t=-0.2$ is necessary to describe half-filled stripes as inferred from the incommensurability.[10] This value is close to the value obtained in a local density approximation study.[68]

(ii) The spin-wave dispersion of the undoped system along the magnetic zone boundary poses a rather stringent constraint on the value of U. In fact, LSWT for the Heisenberg model with only nearest-neighbor exchange interactions $J=4t^2/U$ does not yield any dispersion at all. Only higher order in t/U exchange contributions (cyclic exchange being the most important among them[69–72]) start to produce a dispersion in the magnetic excitations along the magnetic zone boundary, which is therefore very sensitive to the value of U.

We have computed the magnon spectra for the half-filled system within the GA+RPA approach and fitted the spin-wave dispersion of undoped La_2CuO_4 measured at $T=10$ K.[72] As can be seen from Fig. 3, the parameter set $U/t=7.5$ yields excellent agreement with the measured dispersion also along the magnetic zone boundary. The fitting also fixes the overall energy scale $t=342$ meV. This dispersion is in slightly better agreement with experiment than a previous one[67] with $U/t=8$ which was used in Ref. 1 and enhances the already good agreement between theory and

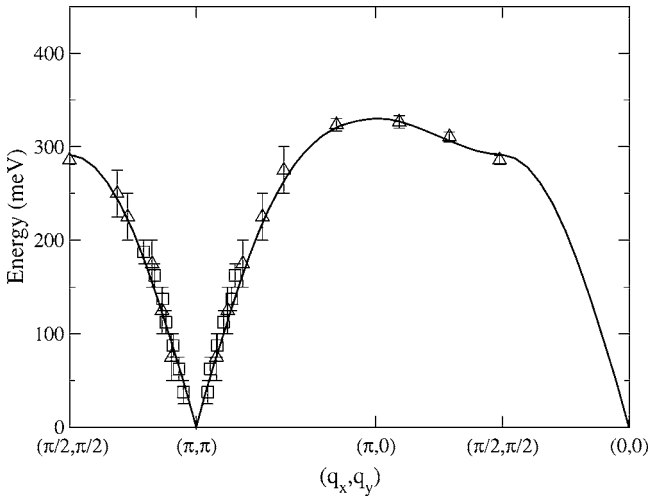

FIG. 3. Energy and wave-vector dependence of magnetic excitations in the half-filled system as obtained from the GA+RPA approach for $U/t=7.5$, $t'/t=-0.2$, and $t=342$ meV. Squares and triangles correspond to data points from INS experiments at $T=10$ K on La_2CuO_4 by Coldea *et al.* (Ref. 72).

experiment for the position of the resonance mode at $n_h=0.125$ discussed below. We note that for $U/t=10$ the fitting in the insulator is significantly worse.[67] All our further calculations are without free parameters. It should be mentioned that a similar estimate for U/t has been obtained from quantum Monte-Carlo calculations of the magnon dispersion[73] and is in the range $U/t\sim 6,8$ obtained from mapping the three-band Hubbard model to the one-band model.[74] Moreover, a similar value of $U/t\sim 8$ has been obtained in a recent fit of the doping dependence of spectral weights in optical data.[75]

Finally, we note that although the present parameter set was optimized with magnetic properties, it also gives reasonable results for charge excitations. Within GA+RPA, one obtains a gap in the optical excitations of 1.8 eV which is close to the 2 eV value of reflectivity experiments.[76]

The saddle-point solutions have been discussed in Ref. 51. Usually we consider stripe textures oriented along the y axis (vertical stripes) where site-centered (SC) and bond-centered (BC) solutions have similar energies. The magnetic unit cell for BC solutions is shown schematically in Fig. 1. Spins are ordered antiferromagnetically in the vertical direction, whereas the ferromagnetic spin alignment between sites at transverse positions 0 and 1 indicates the presence of a domain wall where also doped holes accumulate. In this paper, we label stripes by the horizontal distance d between the hole-rich domain walls, the doping n_h, and the symmetry (BC or SC). In order to compare with experimental data in $La_{2-x}Sr_xCuO_4$ or $La_{2-x}Ba_xCuO_4$, we assume $n_h=x$.

Within the present one-band model calculation we find that the more favorable solutions at small doping are SC but with an energy difference to BC stripes that is negligibly small in large systems. This quasidegeneracy is also found in other one-band calculations.[46–49] On the other hand, BC textures turn out to be more stable in the more accurate three-band Hubbard model[50] and in first-principles computations.[78] Therefore, we pay special attention to BC solutions at low

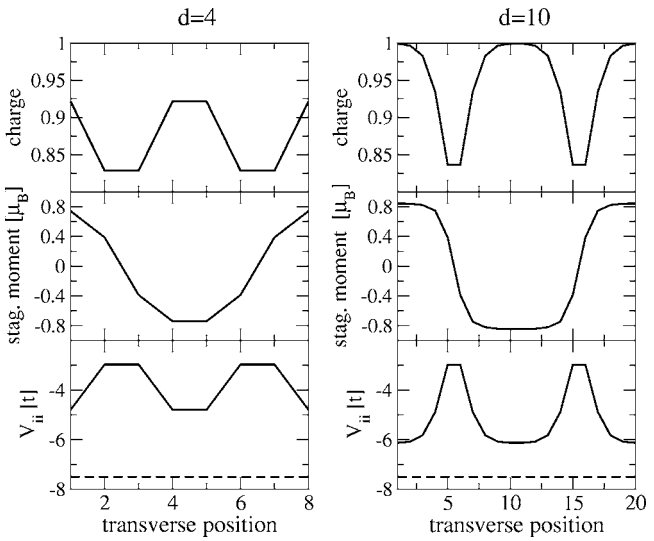

FIG. 4. Profile of the charge (top panels), staggered magnetic order (middle panels), and effective interaction V_{ii} (lowest panels) for $d=4$ and 10 bond-centered stripes in the GA. The dashed line in the lowest panels indicates the "bare" spin interaction of the HF +RPA $V_{ii}^{\mathrm{HF}}=-U/t=-7.5$.

dopings. In the three-band model, the quasidegeneracy appears at slightly larger doping and was related to the anomalous optical properties.[79]

In Fig. 4, we show a cut through the charge (top panels) and staggered magnetic moment profile (central panels) for BC stripe solutions and stripe separation $d=4,10$ evaluated within the GA. For distant stripes ($4d=10$ in Fig. 4), the regions between the domain walls resemble the spin-density wave solution of the undoped system (i.e., $n\approx 1$) whereas doped holes progressively populate the AFM domains when stripes become closer. The moment in the insulating regions is close to $0.8\mu_B$ and is reduced with respect to the full value of $1\mu_B$ due to covalency.[67] This is larger than the expected value in the insulator $\sim 0.6\mu_B$ because we are not including the feedback of the RPA fluctuations on the single-particle expectation values which, for the magnetic moment, are dominated by transverse fluctuations.[62]

The weight of the magnetic Bragg peaks is determined by the Fourier transform of the magnetic moment in the unit cell.[8,67] From the more intense Bragg peak, one can define an "ordered moment." For LCO codoped with Nd it was found[8] that this is about $0.1\mu_B$, whereas the present static GA approach yields $\sim 0.4\mu_B$.[67] Apart from the lack of transverse fluctuations, which may be even more relevant in the stripe phase, it is likely that disorder, not taken into account in our investigation, will depress the weight of Bragg peaks since they require coherence across many unit cells. In this regard it is interesting that estimates from local probes, which are less sensitive to disorder, are much larger and amount to ordered moments of $\sim 0.4\mu_B$.[77] This should be compared with the average of the absolute value of the static moment $m^{\mathrm{GA}}\approx 0.56\mu_B$ obtained within the GA. In this case the overshoot is expected due to the omission of transverse fluctuations.

Obviously the quality of our approach relies on the presence of stripe correlations in the ground state of the Hubbard model. The large clusters needed for clarifying this issue within exact diagonalization methods presently render impossible a solution to the problem. To estimate the quality of the GA with respect to more advanced techniques (which are, however, restricted to smaller clusters and specific boundaries), we have compared the charge distribution with density-matrix renormalization-group (DMRG) calculations[61] on a 7×6 Hubbard cluster doped with four holes and for $U/t=12$. This study also finds metallic stripes. Remarkably the GA charge distribution (omitting RPA fluctuations) is almost identical to the DMRG. In this case the RPA feedback effect is expected to be negligible in the insulator and small in the stripe phase since the lowest energy excitations are gapped in the former and limited to a small phase space in the latter.

The similarity between the exact and the GA charge distribution gives further support to the quality of our starting point solutions in contrast to HF theory, where one finds a qualitatively wrong ground state for realistic parameters.[51] In this regard GA+RPA becomes essential to proceed.

The local part of the effective interaction Eq. (5) (lowest panel in Fig. 4) closely follows the charge modulation. This is in contrast to HF where the effective interaction between spin fluctuations is uniform and given by the bare value of $-U$. We find that the GA modulated interaction is the dominant effect for obtaining a high-energy response in much closer agreement to experimental data, as described below, than the related HF+RPA computations.[40,44,45] The interaction is also strongly renormalized in our approach, one of the reasons why GA+RPA performs much better than HF +RPA upon comparing with exact diagonalization results.[53] It is interesting to notice that the effective value of the interaction we find is close to the value usually taken for the bare interaction in HF+RPA computations ($U\approx 4t$) in order to obtain physically reasonable results.[40,44,45] This phenomenological decrease of U may compensate for some of the inadequacies of HF+RPA producing a theory more similar to GA+RPA.

IV. RESULTS

Figures 5–7 report magnetic excitations for various dopings and stripe separations. The spectra are for selected cuts parallel (right panels) and perpendicular (left panels) to the stripes and correspond to intensity plots of the imaginary part of the transverse magnetic susceptibility times the frequency $\omega\chi_q''(\omega)$. The frequency factor cancels a $1/\omega$ intensity divergence at the Goldstone mode and allows us to visualize all energies with the same intensity scale.

The magnetic excitations for SC and BC stripes are almost identical with only minor differences regarding the intensity distribution and the dispersion as shown in Fig. 6 for $n_h=0.13$. In the other panels, therefore, we only report BC solutions that are more likely to be stable at low doping as discussed above. This similarity is in strong contrast to LSWT calculations for which the spectrum is substantially different.[41,42] Indeed, within LSWT the number of bands is d for BC stripes and $d-1$ for SC stripes. In the latter case, the core spins are assumed to be in $S=0$ states and thus to be

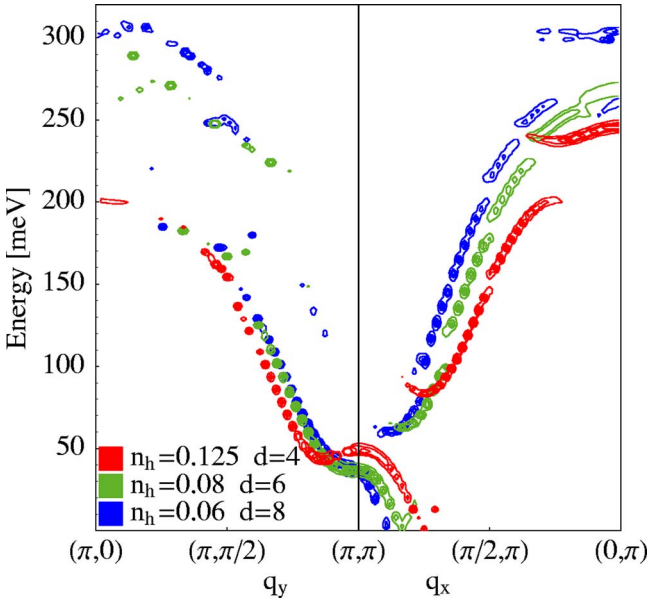

FIG. 5. (Color online) Dispersion of magnetic excitations along the cut $(\pi,0)\rightarrow(\pi,\pi)$ and $(\pi,\pi)\rightarrow(0,\pi)$ for BC stripes and dopings $n_h \leqslant 1/8$ and stripe separation $d \geqslant 4$. The dispersion is obtained from five contours of $\omega\chi_q''(\omega)$ (which is dimensionless) at regular intervals between 0 and 7.

passive. In GA+RPA instead all electrons are active and the number of low-energy magnetic bands is d irrespective of the symmetry of the stripe. (This is not obvious from the figures for large d because the GA+RPA bands have small gaps and are only visible in restricted parts of the Brillouin zone).

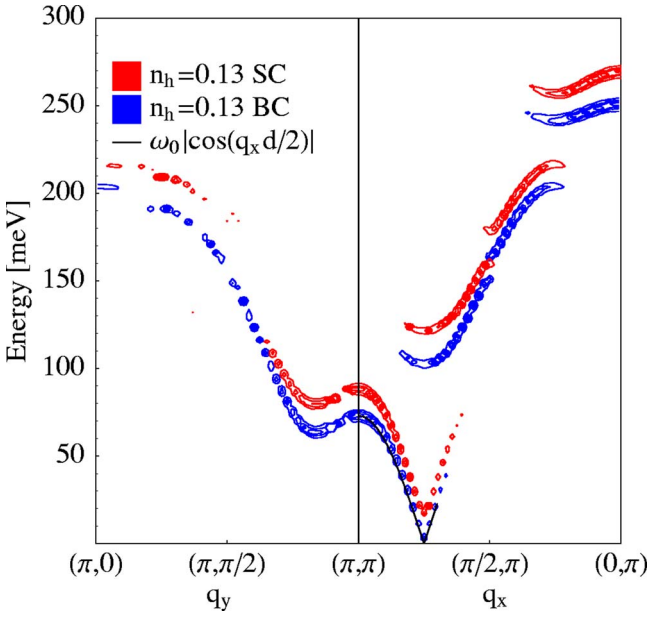

FIG. 6. (Color online) Dispersion of magnetic excitations along the cut $(\pi,0)\rightarrow(\pi,\pi)$ and $(\pi,\pi)\rightarrow(0,\pi)$ for BC and SC stripes and $n_h=0.13$ and stripe separation is $d=4$. The SC data have been shifted by 10 meV for clarity. We also show the fit of the acoustic branch with Eq. (13). The dispersion is obtained from four contours of $\omega\chi_q''(\omega)$ at regular intervals between 0 and 7.

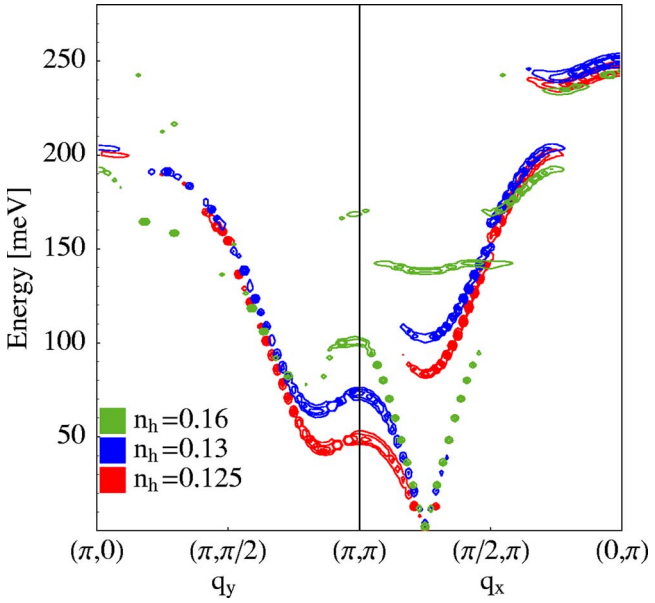

FIG. 7. (Color online) Dispersion of magnetic excitations along the cut $(\pi,0)\rightarrow(\pi,\pi)$ and $(\pi,\pi)\rightarrow(0,\pi)$ for BC stripes at $d=4$ and different dopings. The dispersion is obtained from five contours of $\omega\chi_q''(\omega)$ at regular intervals between 0 and 7.

As expected, a Goldstone mode emerges from the incommensurate wave vector. In GA+RPA, a small gap ($\sim$6 meV) appears in some runs due to convergence problems of the solutions. In these cases we subtract the gap to obtain the physically correct gapless spectra.

The Goldstone mode excitations correspond to long-wavelength transverse fluctuations of the magnetic order parameter, i.e., acoustic spin waves. The dispersion relation consists of a cone around the incommensurate wave vector with an anisotropic intensity distribution. The intersection of the spin-wave cone with the (q_x,ω) plane with $q_y=\pi$ gives rise to two acoustic branches emerging from the incommensurate wave vector $\mathbf{Q}_s$. The large intensity one disperses toward $\mathbf{Q}_{\mathrm{AF}}=(\pi,\pi)$, where it reaches a saddle point ($n_h<0.09$) or a local maximum ($n_h>0.09$). We associate the energy at the AFM wave vector, ω_0, with the resonance energy.[80]

The branch emerging from $\mathbf{Q}_s$ in the cuts and dispersing outwards (i.e., away from $\mathbf{Q}_{\mathrm{AF}}$) rapidly loses intensity with increasing energy. As can be seen from Fig. 5, this effect is more pronounced for large stripe separations. Indeed for $n_h=0.06$ the outward-dispersing branch is hardly visible.

In Fig. 8 we show the LSWT results for $d=8$ and 4 BC stripes with $J_F=0.2$. We can reproduce some qualitative features of the GA+RPA dispersion relation by taking such a small value of J_F as discussed in detail below. The intensity difference effect between the inward- and outward-dispersing Goldstone mode is also observed in the LSWT calculations (Fig. 8), however the difference remains constant as a function of d and is less apparent for large stripe separations.[81]

Since the outward-dispersing branch has not been detected yet, we cannot make a detailed comparison of the relative intensities. Our GA+RPA results suggest that this

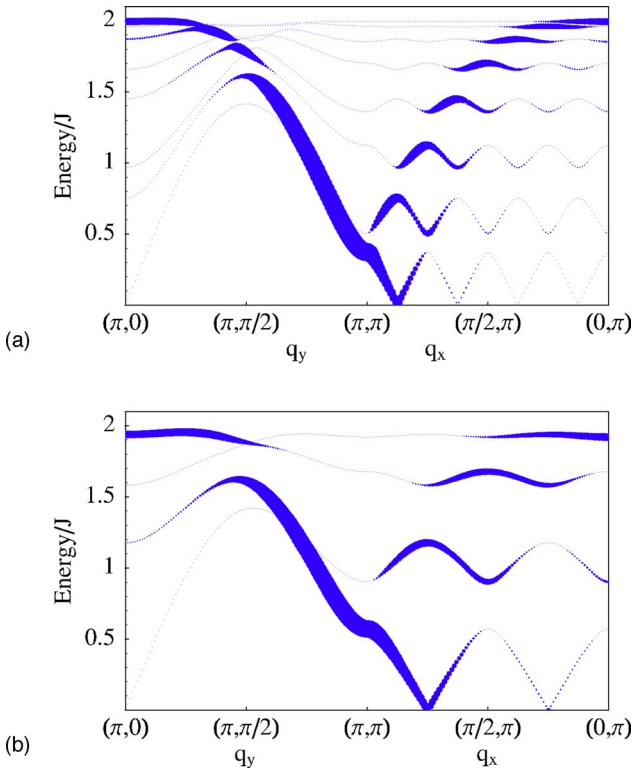

FIG. 8. (Color online) Dispersion of magnetic excitations along the cut $(\pi,0)\rightarrow(\pi,\pi)$ and $(\pi,\pi)\rightarrow(0,\pi)$ for BC stripes oriented along the y direction within LSWT for $d=8$ (top) and $d=4$ (bottom). The radius of the points is proportional to the intensity times the energy of the excitation. Modes with negligible weight are plotted with a small dot. We used a uniform value of the AFM interaction J across all the bonds except for the ferromagnetic bonds where the sign is opposite to ensure stability and the modulus is $J_F=0.2J$ as shown in Fig. 1.

branch should be difficult to observe in the underdoped regime. For example, for $n_h=1/8$ the intrinsic momentum width of the inward branch observed in the experiment will mask the small low-energy region where the outward branch has significant weight (cf. Fig. 11).

For $n_h=0.16$, we expect this problem to be less severe and the branch should become observable, however low-energy INS data[13] do not reveal any signature of the outward-dispersing branch. It may be that our theory overestimates the corresponding intensity in this case or that damping effects, not taken into account in our approach, become dominant. More experimental and theoretical work is needed to clarify this point. It should be mentioned in this regard that HF+RPA calculations[40] suggest a further suppression of the intensity of the outward-dispersing modes from the inclusion of a d-wave order parameter.

The two GA+RPA acoustic branches along the $(q_x,q_y=\pi)$ direction can be fitted by

$$\omega(q_x,\pi)=\omega_0|\cos(q_x d/2)| \tag{13}$$

as shown in Fig. 6. The corresponding velocity perpendicular to the stripe is

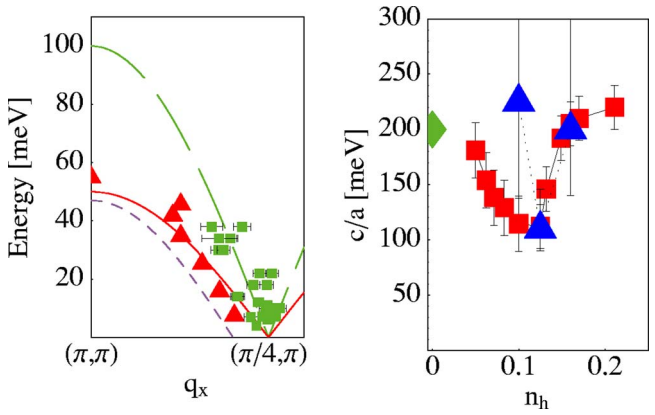

FIG. 9. (Color online) Left panel: Dispersion of magnetic excitations along the cut $(\pi,\pi)\rightarrow(\pi/4,\pi)$ for BC stripes for dopings $n_h=0.1$ (short dashed line), 0.125 (full line), and 0.16 (long dashed line). We include the experimental data from Ref. 11 for $n_h=0.125$ (triangles) and from Ref. 13 for $n_h=0.16$ (squares). Right panel: velocity of the collective mode c divided the lattice spacing a. We report the theoretical result (squares) and the experimental result (triangles) both obtained by fitting Eq. (13) to the data. The diamond at $n_h=0$ is the spin-wave velocity in the insulator.

$$c=\frac{\omega_0 d}{2}. \tag{14}$$

The spin-wave cone is only weakly anisotropic (cf. Figs. 12 and 13) so that the spin-wave velocity along the stripe is not far from this estimate.

In Fig. 9 we show available experimental data for LBCO (Ref. 11) $n_h=0.125$ and LSCO (Ref. 13) $n_h=0.16$ together with the GA+RPA dispersion. There is excellent agreement between theory and experiment for the position of the low-energy acoustic branches and the velocity c of the collective mode. We caution, however, that the errors in the determination of the experimental spin-wave velocity are rather large as shown by the error bars in the right panel of Fig. 9. Even a spin-wave velocity independent of doping is compatible with the present experimental data. To determine the theoretical spin-wave velocity, shown also in the right panel, we used Eqs. (13) and (14). For some runs it was necessary to include a correction to Eq. (13) of the form $\omega_1|\sin(q_x d)|$ with ω_1 in the range ±6 meV. This correction, however, was too noisy due to convergence problems of the runs, so we include this effect as error bars in the theoretical data.

The theoretical velocity as a function of doping has a pronounced minimum at $n_h=1/8$ which seems to be supported by the available experimental data with the mentioned caution on the errors involved.

Inspection of Eq. (14) reveals that at small concentrations the velocity is mainly determined by $d\sim 1/n_h$ due to the weak doping dependence of ω_0 in this regime [cf. Fig. 14(a)]. However, for $n_h>1/8$ the stripe periodicity stays constant ($d=4$) and the rising of ω_0 [cf. Fig. 14(a)] causes the increase of the velocity and thus the appearance of the minimum at $n_h=1/8$. For $n_h=0.1$, the available data for the collective mode[13] (not shown) imply a velocity substantially larger than what we found (as shown in the right panel of

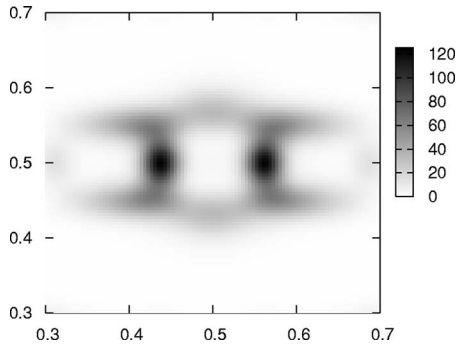

FIG. 10. Contour plot of $\chi''_q(\omega)$ as a function of wave vector for ω=45.6 meV and n_h=0.125. The plot range for the axes is the same as in Fig. 1(c) of Ref. 19. Wave vectors are in units of $2\pi/a$.

Fig. 9). The predicted dispersion is shown in the left panel of Fig. 9 with the dashed line. We expect that the saddle-point energy ω_0 is similar or slightly smaller than at n_h=0.125, whereas the present low-energy experimental data[13] extrapolate to a significantly larger energy. A high-energy experiment should clarify the situation on this point.

For $n_h > 0.09$, the GA+RPA computation additionally shows a "rotonlike" minimum in the direction of the stripe (Figs. 5–7). This effect cannot be explained in LSWT without invoking longer range interactions.

The minimum is located close to $(\pi, 3\pi/4)$, which is equal to $\mathbf{Q}_s$ with x and y directions interchanged. It indicates a tendency of the stripe to develop a spin-density wave with period $8a$ along the stripe. One can speculate that for different parameters the system may develop such an instability resulting in a ground state with a checkerboard pattern as observed on the surface of some compounds.[86]

The maximum at $\mathbf{Q}_{\mathrm{AF}}=(\pi,\pi)$ and the roton minimum give rise to a peak in the momentum integrated structure factor which is slightly lower in energy than the saddle-point "resonance" at the AFM wave vector (Fig. 16). Especially at low doping (i.e., large stripe separations) the excitations around the (π,π) region carry significant weight, which in the integrated spectrum is further enhanced due to the saddle-point structure.

Because of the roton minimum, a constant cut at an energy moderately below the resonance shows intensity both along and perpendicular to the direction of the stripe as shown in Fig. 10. Although our study focuses on LCO, it is remarkable that a similar effect has been recently observed in an untwinned sample array of YBCO by Hinkov and co-workers.[19] The intensity difference between the two directions is also in qualitative agreement with our result.

In Ref. 19, this quasi-two-dimensional distribution of intensity is interpreted as evidence against a "rigid stripe array" which is expected to produce a more anisotropic pattern. It is clear that Ref. 19 cannot be considered as evidence against an *oriented* stripe array since these authors definitively found an asymmetry between x and y directions, i.e., a breaking of C_4 lattice symmetry. As already outlined in the Introduction, the latter can be viewed as the fingerprint of an oriented stripe ground state (in the sense of a "stripe nematic phase"[87]) but may also be due to a structural anisotropy as proposed in Ref. 35. Without further quantitative estimates, one cannot distinguish between both scenarios from Ref. 19.

Our result shows that long-range order with oriented stripes is compatible with a quasi-two-dimensional distribution of intensity between the saddle-point energy and the roton minimum. At lower energies we predict a strongly anisotropic intensity as long as the dispersion is not cutoff by the spin gap. Can we agree with the conclusions of Hinkov and co-workers? This becomes a question of semantics. Our stripes are quite different from the "rigid stripe array" assumed in LSWT since our RPA computation is performed on top of a much softer modulation and also has a much larger phase space for fluctuations, which substantially changes the results. Interpreting "rigid stripe array" in the LSWT sense, we can agree with the statement in Ref. 19 since, as we have shown, LSWT in its simpler form is not able to reproduce this result.

We believe that the fact that our results qualitatively reproduce the observed two-dimensional intensity map observed by Hinkov *et al.* is evidence for the existence of the roton minimum which was obtained[1] before the data of Ref. 19 became available. Naturally, a quantitative comparison should include consideration of the YBCO bilayer structure which would modify the energy of the resonance and may affect intensities. In addition, a description which allows for fluctuating stripes from the start[88] may be more appropriate for YBCO materials since it can capture the appearance of a spin gap. In this regard, some details of our map differ from the experimental data (round shape, external branches) perhaps because of the above reasons. One should keep in mind, however, that the map of Hinkov *et al.*[19] is obtained on the basis of a simple model fitted to four scans in each direction of which only three intersect the ring. Clearly details not considered by their model will not show up. This should be compared with a typical experiment at ISIS as in Refs. 11 and 20 where the maps involve hundreds of scans per direction.

In order to compare with experimental data in twinned samples or for systems in which stripes are stacked orthogonal to each other from one plane to the next, one should average over the two possible orientations of the stripes (vertical and horizontal). Whereas the high-energy magnetic excitations in the direction of the stripes evolve from the saddle point at $\mathbf{Q}_{\mathrm{AF}}$, the spectrum perpendicular to the stripes is composed of several optical branches which are not directly connected to the "resonance." Nevertheless, it is interesting to observe that in GA+RPA the high-energy dispersions parallel and perpendicular to the stripes (Fig. 11) are rather close, indicating an almost isotropic magnetic response at large frequencies. This high-energy "isotropy" is only present up to $n_h \sim 0.15$ where due to the interaction between magnetic domains the optical branches perpendicular to the stripes start to develop a significant gap structure. Figure 11 reveals that also for the optical branches our calculation yields reasonable agreement with the available data.[11] In striking contrast, LSWT (Fig. 8) predicts a series of optical branches in the direction perpendicular to the stripe that are not observed and an anisotropic high-energy response. The GA+RPA high-energy excitations shown in Fig. 11 are slightly displaced toward higher momenta. However, we find excellent agreement for the slope which defines an effective

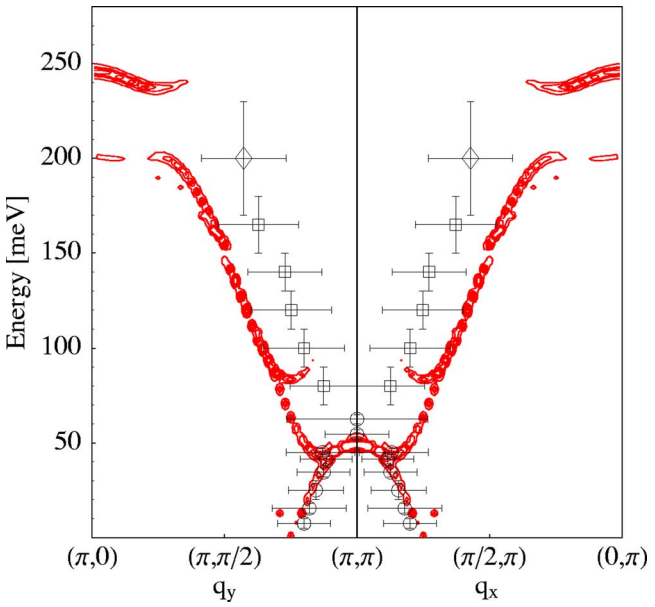

FIG. 11. (Color online) Dispersion of magnetic excitations along the cut $(\pi,0)\rightarrow(\pi,\pi)$ and $(\pi,\pi)\rightarrow(0,\pi)$ for BC stripes at $d=4$ and $n_h=0.125$. We have averaged the data over the two possible orientations of the stripe, vertical and horizontal. The dispersion is obtained from five contours of $\omega\chi''_q(\omega)$ at regular intervals between 0 and 10. We also show the experimental data from Ref. 11 (courtesy of J. Tranquada). The latter horizontal "error" bars indicate the half-width of the peaks, whereas vertical "error" bars indicate an energy interval of data integration.

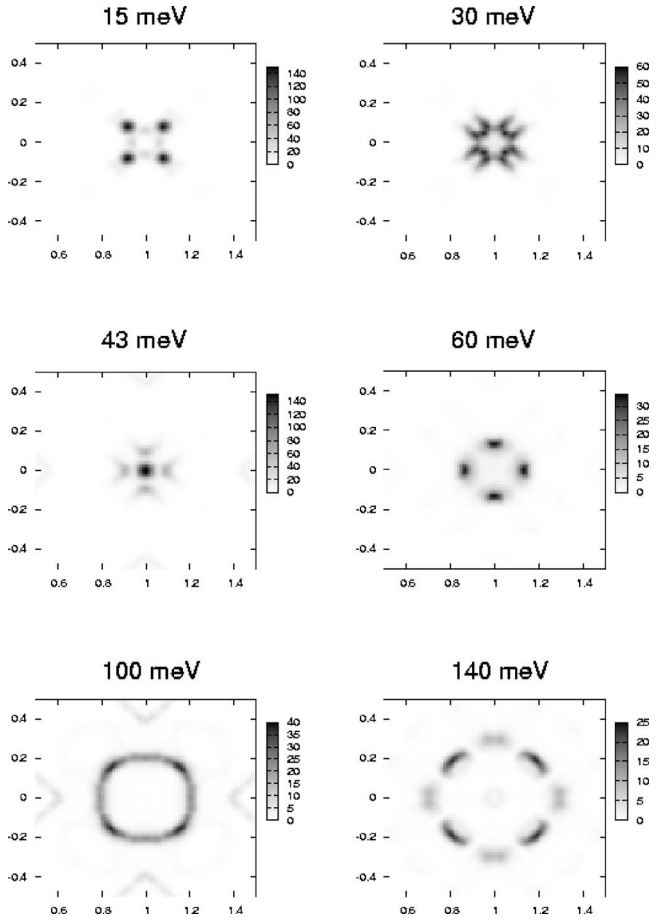

FIG. 12. Contour plots of $\chi''_q(\omega)$ as a function of wave vector at selected energies for doping $n_h=0.08$. The underlying GA solution is a $d=6$ BC stripe array. The wave-vector coordinate system has been rotated by 45° in such a way that the magnetic Brillouin zone of an antiferromagnet occupies all the window of the plot with $\mathbf{Q}_{\mathrm{AF}}=(\pi,\pi)$ at the center. Wave vectors are in units of $2\pi/[\sqrt{(2)}a$.

high-energy spin-wave velocity. The shift of our excitations toward higher momenta may be due to the use of the oversimplified one-band Hubbard model. It would be interesting to see how the high-energy part of the dispersion appears in the three-band Hubbard model.

A quantitative fit to the X-type dispersion shown in Fig. 11 can also be achieved with coupled spin-leg ladder models by fine tuning the interstripe coupling to a quantum critical point.[38] These theories, however, rely on an even charge periodicity of the stripes (as for $n_h=1/8$). In contrast, we obtain qualitatively similar spectra for $n_h=1/8$ ($d=4$) and $n_h=1/10$ ($d=5$) in accord with experiment in LCO.[11,13] On the other hand, our approach cannot be easily generalized to incorporate spin-gapped states as in YBCO which are naturally explained in a ladder picture.[36–39] Another important difference of the ladder scenario with respect to the present work is that at high energies the ladder computation finds propagating modes only in the direction of the stripe, whereas our calculation yields more isotropic spectra in agreement with recent experiments.[93]

Constant energy cuts of the dispersion change shape as the energy of the cuts is increased. We have already shown[1] that our data closely resemble the changes seen in the experiment at $n_h=1/8$.[11] In Figs. 12 and 13 we show contour plots of the transverse susceptibility for a strongly underdoped ($n_h=0.08$) and an almost optimally doped ($n_h=0.16$) system averaged over the two possible orientations of the stripes. In the first case, we consider an underlying $d=6$ BC stripe solution which yields a saddle-point energy at $\omega_0=43$ meV. Below this energy the "resonance feature" splits into the four incommensurate Goldstone modes (from the superposition of vertical and horizontal stripes). The associated spin-wave cones display a strongly asymmetric intensity distribution where the weight is mainly confined in the parts closest to $\mathbf{Q}_{\mathrm{AF}}$ in accord with the intensity difference of the acoustic branches shown in Fig. 5 and discussed above.

Above ω_0, the intensity spreads into a ring-shaped feature which increases with energy. The strongest scattering is on the corners of a square at 15 meV and rotates by 45° at 60 meV resembling the behavior found at $n_h=1/8$ in theory[1] and experiment.[11]

The case of $d=4$ BC stripes at doping $n_h=0.16$ is shown in Fig. 13. The saddle-point energy is at $\omega_0=102$ meV. At low energies, the spin-wave cone displays significant weight in all directions, which leads to the pronounced intensity of the outward-dispersing branch as discussed already in the context of Fig. 7. The complex structure at 87 meV is composed of the incommensurate Goldstone modes and the branch dispersing from $\mathbf{Q}_{\mathrm{AF}}$ toward the roton minimum, which constitute the smaller ring around $\mathbf{Q}_{\mathrm{AF}}$. Additionally one can observe a larger ring whose intensity comes from the

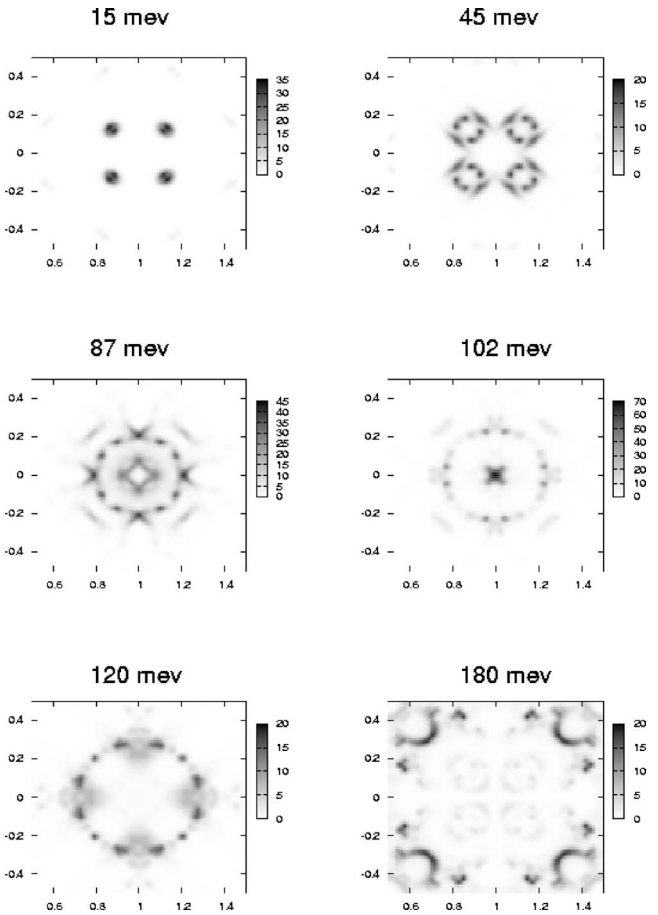

FIG. 13. Contour plots of $\chi''_q(\omega)$ as a function of wave vector at selected energies for doping $n_h=0.16$. The underlying GA solution is a $d=6$ BC stripe array. The wave-vector units are as in Fig. 12.

branch dispersing away from the roton minimum along the stripe direction. A weaker feature along the diagonals originates from the outward-dispersing branches. Above the saddle-point energy, the intensity distribution again forms a ring that increases in diameter with increasing energy.

Figure 14 displays the doping dependence of the resonance frequency and intensity for both BC and SC stripes evaluated within GA+RPA. In the strongly underdoped regime ($0.05 \leqslant n_h \leqslant 1/8$), we find an approximately linear relation $\hbar\omega_0 \approx \alpha + \beta n_h$ with $\beta \approx 250$ meV and $\alpha \approx 20(30)$ meV for BC (SC) stripes in the GA+RPA. Note that for infinitely distant stripes one expects $\omega_0 \to 0$ so that the offset energy α is an artefact of the linear approximation in the considered doping range. A qualitatively similar linear behavior has been found in Ref. 52.

We also show in Fig. 14(a) (full squares) the doping dependence of the resonance energy evaluated within LSWT. We assumed that the doping is given by $n_h=1/(2d)$, which is valid for half-filled stripes with $n_h<1/8$. The energy of the resonance scales in a similar way in both GA+RPA and LSWT for $n_h<1/8$ despite the fact that we take the values of J and J_F as doping-independent. This is not surprising since for $n_h<1/8$ the charge profile of the stripes does not overlap and doping proceeds by varying the distance among the stripes keeping the electronic structure on the core of the

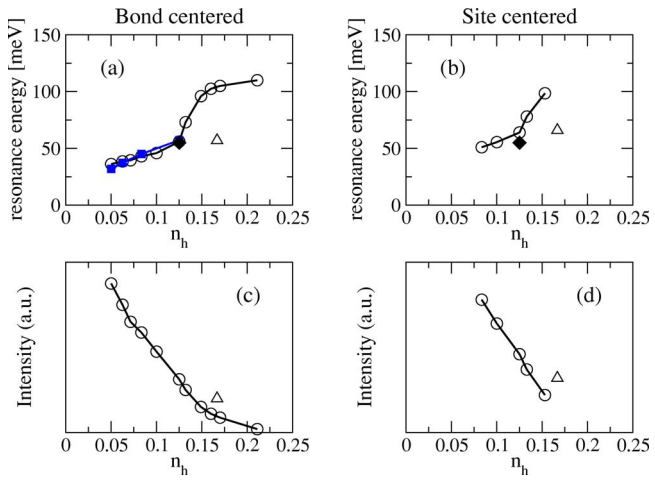

FIG. 14. (Color online) Doping dependence of the resonance frequency and intensity for BC (left panels) and SC (right panels) stripes within the GA+RPA. The circles for $n_h>1/8$ correspond to $d=4$ solutions, whereas the triangle corresponds to the $d=3$ solution. The full diamond symbol is the experimental result from Ref. 11. The full squares in (a) are the LSWT result using $J_F=0.2J$ and $J=100$ meV.

stripe essentially unchanged.[50,51] Therefore, in this respect it makes little difference at low energy to consider the stripes as localized objects as in LSWT with a fixed value of J_F or as more extended objects as in GA+RPA. It is interesting that the effective value of J_F in order to have an overall agreement with the GA+RPA results and with the experiment is quite small, as found in other LSWT studies.[41]

For $n_h>1/8$, effects due to the overlap of the stripe cores become evident. In our previous computations[51,50] within the GA we have found that in this regime it is energetically favorable to add holes into the $d=4$ stripe structure consistent with the doping-independent incommensurability seen in INS experiments.[10] For both BC and SC stripes this leads to a strong increase of the resonance energy and therefore to a deviation from the linear ω_0 versus n_h behavior at low doping. An alternative scenario is phase separation as explained below.

The resonance mode is strongly influenced by the effective magnetic interactions across the domain wall. For example, in the case of a SC stripe depicted in Fig. 15 the spins adjacent to the core site are bridged by an effective AFM interaction J' as it is assumed in LSWT models. The energetics of the resonance mode can be easily understood by adding a small transverse component with momentum $\mathbf{Q}$

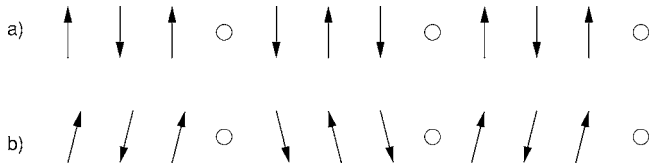

FIG. 15. (a) A schematic cut perpendicular to the stripe through the Néel-type spin structure of $d=4$ SC stripes. (b) Resulting spin structure upon adding transverse spin components $S_\perp \sim \cos(\mathbf{QR})$ with $\mathbf{Q}=(\pi,\pi)$.

$=(\pi,\pi)$ to the domain-wall structure, which provides a simplified picture for the quasiclassical displacements of the spin in the resonance mode as shown in Fig. 15(b). The spins in the AFM regions keep their relative angle constant whereas the angle formed by the spins across the domain wall strongly fluctuates, giving the dominant contribution to the energy of order J'. A similar picture holds for BC stripes with J_F at the place of J'. [In reality, the resonance mode is not completely localized in the domain wall, as suggested by Fig. 15, which makes the dependence on J' (or J_F) more complicated.]

The strong increase of the resonance energy with doping for $n_h \geqslant 1/8$ [Fig. 14(a)] can be understood if the effective value of J_F (J') also increases across the BC (SC) domain walls. As shown in the Appendix , these couplings are dominated by transverse hopping processes of doped holes. The increase of the stripe filling from $\nu=1/2$ for $n_h \geqslant 1/8$ induces a concomitant enhancement of J_F (J') explaining the behavior of the upper panels of Fig. 14.

Since upon doping the saddle-point energy for $n_h < 1/8$ increases more slowly than the experimental T_c, our calculations predict a nonconstant ratio between ω_0 and kT_c in the underdoped regime of LCO. This ratio decreases from $\omega_0/kT_c \approx 27$ for $n_h=0.05$ to $\omega_0/kT_c \approx 17$ for $n_h=1/8$. This is significantly larger than the resonance energy to kT_c ratio ~ 5.4 as obtained for YBCO. Therefore, if the saddle-point excitation is important for the superconducting mechanism, its effect on T_c is modulated by other factors.

In LCO materials, the only experimental value for ω_0 available up to now[11] (shown as the full diamond in Fig. 14) falls exactly on the curve for BC stripes, whereas it is slightly below the $\omega_0(1/8)$ result for SC ones. Although the difference is too small to be conclusive (given the approximations involved), the fact that BC stripes give the best fit is in agreement with our previous finding within the three-band model[50] that BC stripes are the more stable textures in the underdoped regime of LCO cuprates.

One can obtain two more points for the resonance energy by extrapolating the experimental data of Ref. 13 with the aid of Eq. (13). One obtains a similar result as in the right panel of Fig. 9. The extrapolated experimental resonance is in good agreement with theory for $n_h=0.16$, whereas it is at much higher energies for $n_h=0.1$.

Around optimal doping, one finds a proliferation of mean-field solutions with energy similar to stripes probably indicating a melting of these textures. Therefore, in this regime the nature of the ground state is less clear. Restricting to vertical stripes, we find a transition toward $d=3$ stripes both in the one-[51] and three-band[50] model at $n_h=0.19-0.24$. Experimentally the incommensurability ε for doping $n_h > 1/8$ has been determined for LSCO (Ref. 10) and LCO codoped with Nd.[9] In the former material, $\varepsilon \approx 0.125$ up to $n_h=0.25$ whereas for the latter compound the incommensurability reaches $\varepsilon \approx 0.15$ for $n_h=0.2$, which is compatible with $d=3$ stripes. For this solution, the resonance frequency and intensity are shown with a triangle in Fig. 14. Clearly, more measurements of the dispersion and in particular the resonance at doping $n_h > 1/8$ will clarify the situation.

In Fig. 16, we show the density of magnetic excitations

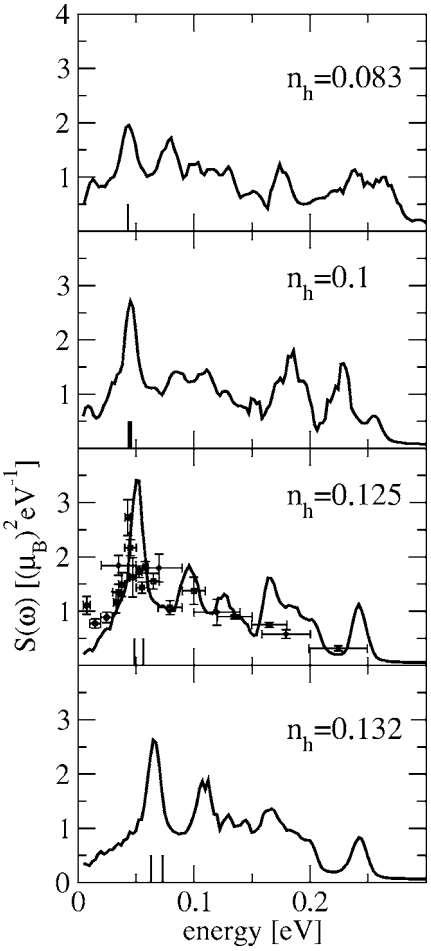

FIG. 16. Density of magnetic excitations $S(\omega)$ (see text) for three doping levels $n_h=0.083$, 0.1, 0.125, and 0.132. Theoretical curves include a factor $Z_d\eta_\perp=0.25$. The vertical bars indicate the energies of the saddle point at $\mathbf{Q}_{\mathrm{AF}}$ and the roton-type minimum in the dispersion along the stripes. Experimental data for $n_h=0.125$ are from Ref. 11.

$$S(\omega) = \frac{1}{N}\sum_q {}' S_q^{\mathrm{eff}}(\omega). \tag{15}$$

Here the sum is restricted to the magnetic Brillouin zone for commensurate AF order to conform to the usual experimental practice and N denotes the number of lattice sites.

As doping increases, spectral weight is transfered from high energy to the resonance region in good agreement with experiment.[67,83] The increase of weight around the resonance energy is not a matrix element but a density of states effect. Indeed, the intensity at the resonance decreases with doping (Fig. 14), which, however, is overcompensated for by the strong Van Hove singularity produced by the saddle-point-like dispersion around (π,π). We have performed preliminary calculations of $S(\omega)$ for $n_h < 0.05$, where stripes are diagonal, which in fact indicate that at very low doping the density of magnetic excitations acquires again the characteristics of the undoped AFM.

For $n_h > 0.09$, both the roton minimum and the saddle point ("resonance") contribute to the peak. The correspond-

ing energies are marked as vertical bars in the panels of Fig. 16. At $n_h=0.1$, both energies almost coincide and give rise to the peak in $S(\omega)$ at $\omega=45$ meV, whereas for higher dopings they are clearly separated. At $n_h=0.125$, the overall structure of $S(\omega)$ consists of a dominant peak around the "resonance" frequency and several humps at higher energy arising from the optical bands. We obtain good agreement with the absolute intensity of the experiment Ref. 11 by choosing $Z_d\eta_\perp \approx 0.25$ [cf. Eq. (12)], which is in good agreement with the estimates of Ref. 67.

V. CONCLUSIONS

In this paper, we have studied the doping dependence of spin excitations in high-T_c materials of the LCO type based on a stripe picture. The necessity for an understanding of these excitations is suggested by the direct relation found between incommensurate scattering parallel to the Cu-O bond and superconductivity in LCO compounds.[14,15]

The comparison with the limited experimental data available so far gives good agreement for both acoustic low-energy magnons and the high-energy optical spin excitations. Also the absolute intensity of the modes is in reasonable agreement with experiment taking into account the results of Ref. 67. The fact that we can reconcile our computations with experiments is remarkable given the simplicity of the Hamiltonian and the fact that the three model parameters U, t, and t' are fixed by strong constraints prior to the computations of spin excitations in the doped phase.

We provide a nontrivial prediction for the dependence of the velocity of the acoustic spin-wave mode and the energy of the saddle point on doping. The spin-wave velocity has a dip at $n_h=1/8$ which coincides with a similar anomaly seen in the doping dependence of T_c.[84,85] Although the superconducting anomaly is probably related to charge ordering along the stripe, the coincidence is intriguing.

The nature of the ground state is not so clear as one approaches the overdoped regime since one has to take into account the melting of the stripes, and non-Gaussian fluctuation effects beyond RPA will become important. Also it is conceivable that phase separation between the underdoped stripes and an overdoped Fermi liquid occurs as mentioned in Ref. 50. Since we assume a uniform stripe phase, one can find evidence in favor of or against this scenario by studying the doping dependence of the saddle-point energy. In the phase separation scenario, we would expect that at some point the population of the domain walls by holes saturates, thus hampering a further increase of the saddle-point energy with doping.

The GA+RPA results turn out to be considerably different from the predictions of LSWT, however it is interesting that some features can be qualitatively reproduced by this simple theory. These include (i) the difference in intensity among the two acoustic branches emerging from the incommensurate point,[81] (ii) the strong intensity at the saddle point associated with the resonance, (iii) the fact that the first optical branch in the direction perpendicular to the stripe is separated from the acoustic branch at (π,π), and (iv) the doping dependence of the resonance energy for $n_h \leqslant 1/8$ as shown in Fig. 14.

Regarding the differences between LSWT and GA+RPA, the most notable ones are the absence of the roton minimum in LSWT and the different number of bands among SC and BC dispersions in LSWT versus the similarity of the dispersion for the two symmetries in GA+RPA. Moreover, we have found that the dispersion of the optical branches perpendicular to the stripes differs significantly between GA+RPA and LSWT. For example, upon comparing Figs. 7 and 8 it turns out that the first optical branch is inverted with respect to its mean energy.

Within LSWT, the coupling between adjacent AFM domains is described by an effective ferromagnetic exchange J_F in the case of BC stripes (or an AFM coupling J' for SC textures). It is interesting that the effective value of J_F (J'), in order to have an overall agreement with the GA+RPA results and with experiment, is quite small as found in other LSWT studies.[41] With this small value, one may wonder whether the magnetic system has long-range order at all or whether it is disordered due to quantum fluctuations.[41] In any case, we expect the system to be close to a magnetic quantum critical point. This is in agreement with the experimental results of Aeppli and collaborators, which indeed see nearly quantum critical behavior close to the incommensurate wave vectors.[82]

Regarding the RPA approach that assumes a uniform Fermi liquid as a starting point,[27–35] it has the advantage that it does not break C_4 lattice symmetry nor SU(2) spin rotational symmetry in agreement with what one expects in overdoped materials. On the other hand, since the starting point is a Fermi liquid this approach cannot be pushed to the dilute regime or to energies of the order of the charge-transfer gap, i.e., describe charge excitations across the Hubbard bands. Within this scheme one obtains a dispersion relation for spin excitations that differs considerably from ours. For example, there is no optical branch that continuously merges with the saddle point.[33,34] Also the low-energy response never separates into four spots in momentum space as the spin-wave cones for a striped system. Instead the incommensurate spin response forms a two-dimensional structure at very low energies. Also the integrated spectral weight is concentrated in a much smaller energy range.[29] Finally, for untwinned systems spectral weight is expected to appear in both directions with some modulation due to structural anisotropy,[35] whereas in our theory at the lowest energies practically all the weight is in the direction perpendicular to the stripes.

The natural question that arises is whether the results of the present investigation may also be relevant for an understanding of spin excitations in YBCO. The acoustic dispersion shows a low-energy spin gap ($\Delta \sim 30$ meV at optimal doping) and thus does not reach the incommensurate wave vector at $\omega=0$. In this case it is more likely that the system is in a quantum disordered spin phase as suggested by the ladder theories.[36,37,39] One expects that the system shows short-range order with a correlation length of the order of $\Delta/(\hbar c) \sim 5a$ and that for energies larger than Δ the response of the system resembles that of an ordered phase. For this reason, one can expect that a computation such as the present one is suitable for a description of the universal high-energy spin response.[11,13,20] One encounters a similar situation in the one-dimensional Hubbard model for large U where a com-

putation of RPA fluctuations on top of a spin-density wave will in many respect be in better agreement with the exact solution (which has no long-range order) than RPA fluctuations on top of a homogeneous Slater determinant. Alternatively, a scenario of fluctuating stripes where also the charge loses its long-range order can capture the effect of a spin gap.[88] One has to keep in mind, however, that too many orientational fluctuations can result in an isotropic state, which is not what is found in the experiment of Ref. 19.

In YBCO, one finds an apparent correlation between the resonance frequency and T_c in the sense that both display a similar parabolic shape as a function of doping so that $\omega_0 \approx 5.3kT_c$.

Measurements of ω_0 have been performed from 7% underdoping up to 2% overdoping (see, e.g., Refs. 5 and 16). Due to the spin gap it is more difficult to extract the behavior of the incommensurability from the data. The authors in Ref. 16 find that ϵ already saturates for doping $n_h \approx 0.1$ compatible with a stripe spacing of $d=5$ (extrapolation to $\omega=0$ implies a larger incommensurability similar to LCO). It is then reasonable to assume that the saturation corresponds to the situation in which holes are doped into a stripe structure with fixed distance as in the case of LCO for $n_h > 1/8$.

We find that the resonance energy as a function of doping tends to have a saturation or a slower rate of growth with doping in the underdoped and the overdoped regime [Fig. 14(a)]. This is compatible with Fig. 29 in Ref. 16, which reports a flattening of the ω_0 versus T_c relation for both optimally doped and strongly underdoped samples. In the latter case, this would correspond to the transition toward the regime where stripes are created at distances $d > 5$.

Finally our investigations suggest an explanation for the apparent two-dimensional magnetic scattering below the resonance in detwinned samples of YBCO.[19] Arguments against a "rigid" stripe in this compound are based on the assumption that in a detwinned material stripes preferably align in the direction of the CuO chains running along the b^* direction. From spin-only stripe models[36,37,41,42] one then expects a low-energy magnetic response only in the a^* direction. Instead, the experimental data[18,19] show an anisotropic intensity modulation with maxima along the a^* direction but also significant weight along b^*. Lateral fluctuations of the stripes,[89] which in our harmonic RPA approach are present[79] but decoupled from the magnetic modes, can also explain this result. On the other hand, our present computations show that the observed two-dimensional but anisotropic intensity modulation can be explained by the rotonlike minimum in the dispersion. In addition, our spectra display an almost isotropic response for energies well above the saddle point, in agreement with neutron scattering results on a detwinned and underdoped YBCO sample by Stock and co-workers.[92] The calculation of magnetic excitations from stripes within the time-dependent GA therefore yields a nontrivial crossover from one-dimensional behavior at low energies to a quasi-two-dimensional response at high energies with an intermediate anisotropic but two-dimensional structure at the roton minimum. In contrast, spin-only models yield a one-dimensional spectrum over the whole range of energies.

After this work was submitted and posted,[91] new INS data for an untwinned sample array of YBCO became available.[93] In our opinion, the strong anisotropy found at the lowest energies is incompatible with uniform Fermi liquid theories. In contrast, some of our predictions based on stripes are qualitatively reproduced. Above the resonance the intensity is similar for both directions in qualitative agreement with Figs. 5–7 and in disagreement with the ladder theories.[36–38] Moderately below the resonance there is intensity in both directions, whereas at lower energies the intensity becomes much more anisotropic [cf. Figs. 2(a) and 2(b) of Ref. 93], which is qualitatively consistent with a roton minimum. On the other hand, our computations do not include superconductivity, temperature effects, and damping, which are clearly important in the experiments. In addition, specific computations for bilayer systems are in progress in order to investigate the relevance of our results for YBCO materials more quantitatively.

ACKNOWLEDGMENTS

G.S. acknowledges financial support from the Deutsche Forschungsgemeinschaft and the Japanese Society for the Promotion of Science for enabling a research visit at the IMR, Sendai where this work was completed. We are grateful to S. Maekawa and T. Tohyama for stimulating discussions, and especially to M. Fujita, K. Yamada, J. Tranquada, N. B. Christensen, D. McMorrow, and B. Keimer for imparting knowledge on their experiments.

APPENDIX: DOPING DEPENDENCE OF THE MAGNETIC COUPLING ACROSS STRIPES

In this appendix, we present simple arguments to show how the filling of the domain walls by holes for $n_h > 1/8$ affects the effective magnetic interaction across the stripe. Our arguments will be based on strong coupling and we decouple the motion of charge carriers perpendicular and along the domain walls. The kinetic energy gain of the latter is responsible for the stability of $\nu=1/2$ half-filled stripes.[51] In the following, ν is fixed and we concentrate on the transverse motion which gives rise to the magnetic coupling between antiphase AFM domains.

SC stripes. For half-filled stripes ($n_h < 1/8$), the core will be essentially in a mixture of configurations of the kind

$$\uparrow 0 \downarrow (50\%),$$

$$\uparrow\uparrow\downarrow (25\%),$$

$$\uparrow\downarrow\downarrow (25\%),$$

where we have represented three sites perpendicular to the stripe, the central one corresponding to the core. 0 denotes a hole and we focused on three sites in which the prevailing configuration of the external spins is $\uparrow$ and $\downarrow$. Since for half-filled stripes a hole occupies a core site with probability 50%, the absence of a hole implies the presence of an up or down spin with probability 25%, respectively. One can draw a similar picture in the case in which the prevailing configuration of the external spins is $\downarrow$ and $\uparrow$. The hole in the core favors the AFM coupling of the adjacent spins through

virtual processes of the kind 0 2 0, where 2 denotes a doubly occupied site. Therefore, the gradual population of the core with holes for $n_h > 1/8$ should enhance the coupling J' thus leading to an increase of the resonance energy as discussed in Sec. IV.

BC stripes. Stability of the structure requires that the core be composed of two sites which are coupled by an effective ferromagnetic interaction J_F. The core spins are coupled by an effective antiferromagnetic exchange J to the external spins. For the case in which the prevailing configuration of the external spins is $\downarrow$ and $\downarrow$ (like in the upper row of Fig. 1), one has for a half-filled stripe the typical configurations

$$\downarrow 0 \uparrow \downarrow (25\%),$$

$$\downarrow \uparrow 0 \downarrow (25\%),$$

$$\downarrow \uparrow \uparrow \downarrow (50\%).$$

The first two configurations favor the antiphase alignment through processes of the kind 0 2 0 $\downarrow$ and $\downarrow$ 0 2 0. Since these process involve holes, one expects an increase of the effective J_F when the numbers of holes in the domain wall starts to deviate from half-filling for $n_h > 1/8$.

[1] G. Seibold and J. Lorenzana, Phys. Rev. Lett. **94**, 107006 (2005).
[2] Rossat-Mignod *et al.*, Physica C **185**, 86 (1991).
[3] P. Bourges, L. P. Regnault, Y. Sidis, and C. Vettier, Phys. Rev. B **53**, 876 (1996).
[4] P. Dai, H. A. Mook, S. M. Hayden, G. Aeppli, T. G. Perring, R. D. Hunt, and F. Doğan, Science **284**, 1344 (1999).
[5] P. Bourges, B. Keimer, S. Pailhes, L. P. Regnault, Y. Sidis, and C. Ulrich, Physica C **424**, 45 (2005).
[6] S. Pailhès, Y. Sidis, P. Bourges, V. Hinkov, A. Ivanov, C. Ulrich, L. P. Regnault, and B. Keimer, Phys. Rev. Lett. **93**, 167001 (2004).
[7] J. M. Tranquada, B. J. Sternlieb, J. D. Axe, Y. Nakamura, and S. Uchida, Nature (London) **375**, 561 (1995).
[8] J. M. Tranquada, J. D. Axe, N. Ichikawa, Y. Nakamura, S. Uchida, and B. Nachumi, Phys. Rev. B **54**, 7489 (1996).
[9] J. M. Tranquada, J. D. Axe, N. Ichikawa, A. R. Moodenbaugh, Y. Nakamura, and S. Uchida, Phys. Rev. Lett. **78**, 338 (1997).
[10] K. Yamada, C. H. Lee, K. Kurahashi, J. Wada, S. Wakimoto, S. Ueki, H. Kimura, Y. Endoh, S. Hosoya, G. Shirane, R. J. Birgeneau, M. Greven, M. A. Kastner, and Y. J. Kim, Phys. Rev. B **57**, 6165 (1998).
[11] J. M. Tranquada, H. Woo, T. G. Perring, H. Goka, G. D. Gu, G. Xu, M. Fujita, and K. Yamada, Nature (London) **429**, 534 (2004).
[12] M. Fujita, H. Goka, K. Yamada, J. M. Tranquada, and L. P. Regnault, Phys. Rev. B **70**, 104517 (2004).
[13] N. B. Christensen, D. F. McMorrow, H. M. Rønnow, B. Lake, S. M. Hayden, G. Aeppli, T. G. Perring, M. Mangkorntong, M. Nohara, and H. Tagaki, Phys. Rev. Lett. **93**, 147002 (2004).
[14] S. Wakimoto, H. Zhang, K. Yamada, I. Swainson, Hyunkyung Kim, and R. J. Birgeneau, Phys. Rev. Lett. **92**, 217004 (2004).
[15] S. Wakimoto, G. Shirane, Y. Endoh, K. Hirota, S. Ueki, K. Yamada, R. J. Birgeneau, M. A. Kastner, Y. S. Lee, P. M. Gehring, and S. H. Lee, Phys. Rev. B **60**, R769 (1999).
[16] P. Dai, H. A. Mook, R. D. Hunt, and F. Doğan, Phys. Rev. B **63**, 054525 (2001).
[17] H. A. Mook, P. Dai, and F. Doğan, Phys. Rev. Lett. **88**, 097004 (2002).
[18] H. A. Mook, P. Dai, F. Doğan, and R. Hunt, Nature (London) **404**, 729 (2000).
[19] V. Hinkov, S. Pailhés, P. Bourges, Y. Sidis, A. Ivanov, A. Kulakov, C. Lin, D. Chen, C. Bernhard, and B. Keimer, Nature (London) **430**, 650 (2004).
[20] S. M. Hayden, H. A. Mook, P. Dai, T. G. Perring, and F. Doğan, Nature (London) **429**, 531 (2004).
[21] H. M. Rønnow, L. P. Regnault, C. Ulrich, B. Keimer, M. Ohl, P. Bourges, and Y. Sidis, *ILL Annual Report 2000* (Institut Laue-Langevin, Grenoble, 2000), p. 18.
[22] M. Arai, T. Nishijima, Y. Endoh, T. Egami, S. Tajima, K. Tomimoto, Y. Shiohara, M. Takahashi, A. Garrett, and S. M. Bennington, Phys. Rev. Lett. **83**, 608 (1999).
[23] C. Stock, W. J. L. Buyers, R. Liang, D. Peets, Z. Tun, D. Bonn, W. N. Hardy, and R. J. Birgeneau, Phys. Rev. B **69**, 014502 (2004).
[24] D. Reznik, P. Bourges, L. Pintschovius, Y. Endoh, Y. Sidis, T. Masui, and S. Tajima, Phys. Rev. Lett. **93**, 207003 (2004).
[25] H. F. Fong, P. Bourges, Y. Sidis, L. P. Regnault, A. Ivanov, G. D. Gu, N. Koshizuka, and B. Keimer, Nature (London) **398**, 588 (1999).
[26] H. He, P. Bourges, Y. Sidis, C. Ulrich, L. P. Regnault, S. Pailhes, N. S. Berzigarova, N. N. Kolesnikov, and B. Keimer, Science **295**, 1045 (2002).
[27] Y.-J. Kao, Q. Si, and K. Levin, Phys. Rev. B **61**, R11898 (2000).
[28] J. Brinckmann and P. A. Lee, Phys. Rev. Lett. **82**, 2915 (1999).
[29] M. R. Norman, Phys. Rev. B **61**, 14751 (2000).
[30] F. Onufrieva and P. Pfeuty, Phys. Rev. B **65**, 054515 (2002).
[31] S. Iikubo, M. Ito, A. Kobayashi, M. Sato, and K. Kakurai, J. Phys. Soc. Jpn. **74**, 275 (2005).
[32] M. Ito, S. I. Y. Yasui, M. Soda, A. Kobayashi, M. Sato, K. Kakurai, C.-H. Lee, and K. Yamada, J. Phys. Soc. Jpn. **73**, 991 (2004).
[33] A. P. Schnyder, A. Bill, C. Mudry, R. Gilardi, H. M. Rønnow, and J. Mesot, Phys. Rev. B **70**, 214511 (2004).
[34] I. Eremin, D. K. Morr, A. V. Chubukov, K. Bennemann, and M. R. Norman, Phys. Rev. Lett. **94**, 147001 (2005).
[35] I. Eremin and D. Manske, Phys. Rev. Lett. **94**, 067006 (2005).
[36] M. Vojta and T. Ulbricht, Phys. Rev. Lett. **93**, 127002 (2004).
[37] G. S. Uhrig, K. P. Schmidt, and M. Grüninger, Phys. Rev. Lett. **93**, 267003 (2004).
[38] G. S. Uhrig, K. P. Schmidt, and M. Grüninger, J. Magn. Magn. Mater. **290**, 330 (2005)
[39] G. S. Uhrig, K. P. Schmidt, and M. Grüninger, J. Phys. Soc. Jpn. **74**, 86 (2005).
[40] B. M. Andersen and P. Hedegård, Phys. Rev. Lett. **95**, 037002 (2005).
[41] F. Krüger and S. Scheidl, Phys. Rev. B **67**, 134512 (2003).

[42] E. W. Carlson, D. X. Yao, and D. K. Campbell, Phys. Rev. B **70**, 064505 (2004).
[43] A recent calculation within a projection formalism for the *tJ* model[90] is more promising in this regard.
[44] M. I. E. Kaneshita and K. Machida, J. Phys. Soc. Jpn. **70**, 866 (2001).
[45] M. I. E. Kaneshita, R. Morino, and K. Machida, J. Phys. Chem. Solids **63**, 1545 (2002).
[46] S. R. White and D. J. Scalapino, Phys. Rev. Lett. **80**, 1272 (1989).
[47] S. R. White and D. J. Scalapino, Phys. Rev. Lett. **81**, 3227 (1998).
[48] M. Fleck, A. I. Lichtenstein, E. Pavarini, and A. M. Oleś, Phys. Rev. Lett. **84**, 4962 (2000).
[49] M. Fleck, A. I. Lichtenstein, and A. M. Oleś, Phys. Rev. B **64**, 134528 (2001).
[50] J. Lorenzana and G. Seibold, Phys. Rev. Lett. **89**, 136401 (2002).
[51] G. Seibold and J. Lorenzana, Phys. Rev. B **69**, 134513 (2004).
[52] C. D. Batista, G. Ortiz, and A. V. Balatsky, Phys. Rev. B **64**, 172508 (2001).
[53] G. Seibold and J. Lorenzana, Phys. Rev. Lett. **86**, 2605 (2001).
[54] G. Seibold, F. Becca, P. Rubin, and J. Lorenzana, Phys. Rev. B **69**, 155113 (2004).
[55] T. Li, P. Wölfle, and P. J. Hirschfeld, Phys. Rev. B **40**, 6817 (1989).
[56] R. Frésard and P. Wölfle, Int. J. Mod. Phys. B **6**, 237 (1992).
[57] M. Bak and R. Micnas, J. Phys.: Condens. Matter **10**, 9029 (1998).
[58] F. Gebhard, Phys. Rev. B **41**, 9452 (1990).
[59] G. Kotliar and A. E. Ruckenstein, Phys. Rev. Lett. **57**, 1362 (1986).
[60] We indicate the lattice associated with the stripe solution by a superlattice to distinguish it from the underling fundamental lattice generated by $\mathbf{A}_1=(1,0)$ and $\mathbf{A}_2=(0,1)$.
[61] S. R. White and D. J. Scalapino, Phys. Rev. Lett. **91**, 136403 (2003).
[62] J. R. Schrieffer, X. G. Wen, and S. C. Zhang, Phys. Rev. B **39**, 11663 (1989).
[63] Within our scheme, the RPA corresponds to the small-amplitude approximation for oscillations around the GA saddle point, in which case the particle-hole matrix elements of $\rho_{i\sigma,j\sigma}$ may be chosen to be independent coordinates. A full-time-dependent treatment would also imply the coupling with pairing correlations which is neglected in the RPA (see, e.g., Refs. 64 and 65).
[64] P. Ring and P. Schuck, *The Nuclear Many-Body Problem* (Springer-Verlag, New York, 1980).
[65] J. Blaizot and G. Ripka, *Quantum Theory of Finite Systems* (MIT Press, Cambridge, MA, 1986).
[66] S. W. Lovesey, *Theory of Neutron Scattering from Condensed Matter* (Clarendon Press, Oxford, 1984).
[67] J. Lorenzana, G. Seibold, and R. Coldea, Phys. Rev. B **72**, 224511 (2005).
[68] E. Pavarini, I. Dasgupta, T. Saha-Dasgupta, O. Jepsen, and O. K. Andersen, Phys. Rev. Lett. **87**, 047003 (2001).
[69] M. Takahashi, J. Phys. C **10**, 1289 (1977).
[70] M. Roger and J. M. Delrieu, Phys. Rev. B **39**, 2299 (1989).
[71] J. Lorenzana, J. Eroles, and S. Sorella, Phys. Rev. Lett. **83**, 5122 (1999).
[72] R. Coldea, S. M. Hayden, G. Aeppli, T. G. Perring, C. D. Frost, T. E. Mason, S.-W. Cheong, and Z. Fisk, Phys. Rev. Lett. **86**, 5377 (2001).
[73] P. Sengupta, R. T. Scalettar, and R. R. P. Singh, Phys. Rev. B **66**, 144420 (2002).
[74] H. B. Schüttler and A. J. Fedro, Phys. Rev. B **45**, 7588 (1992).
[75] T. Tohyama, Y. Inoue, K. Tsutsui, and S. Maekawa, Phys. Rev. B **72**, 045113 (2005).
[76] S. Uchida, T. Ido, H. Takagi, T. Arima, Y. Tokura, and S. Tajima, Phys. Rev. B **43**, 7942 (1991).
[77] G. B. Teitel'baum, I. M. Abu-Shiekah, O. Bakharev, H. B. Brom, and J. Zaanen, Phys. Rev. B **63**, 020507(R) (2000).
[78] V. I. Anisimov, M. A. Korotin, A. S. Mylnikova, A. V. Kozhevnikov, D. M. Korotin, and J. Lorenzana, Phys. Rev. B **70**, 172501 (2004).
[79] J. Lorenzana and G. Seibold, Phys. Rev. Lett. **90**, 066404 (2003).
[80] This is a simplification since we are neglecting damping effects. In a more accurate computation, the saddle-point mode will overlap with particle-hole excitations, making the mode much broader. The temperature-dependent opening of a gap in the fluctuation spectrum of these second bosonic modes may produce the appearance of a sharp resonance at a smaller energy, which may be more properly called "the resonance." Since these effects are not present in our computation, we do not distinguish between the saddle-point energy and the resonance energy.
[81] The difference in intensity is not so obvious in the presentation of the results in Refs. 41 and 42 due to the different way of plotting the data. The weight diverges as $1/\omega$ at low frequency and saturates within the intensity scale of Refs. 41 and 42. Our choice of plotting $\omega\chi_q''(\omega)$ avoids this problem and the difference in intensity becomes evident.
[82] G. Aeppli, T. E. Mason, S. M. Hayden, H. A. Mook, and J. Kulda, Science **278**, 1432 (1997).
[83] S. M. Hayden, G. Aeppli, H. A. Mook, T. G. Perring, T. E. Mason, S.-W. Cheong, and Z. Fisk, Phys. Rev. Lett. **76**, 1344 (1996).
[84] A. R. Moodenbaugh, Y. Xu, M. Suenaga, T. J. Folkerts, and R. N. Shelton, Phys. Rev. B **38**, 4596 (1988).
[85] M. K. Crawford, W. E. Farneth, E. M. M. III, R. L. Harlew, and A. H. Moudden, Science **250**, 1390 (1989).
[86] T. Hanaguri, C. Lupien, Y. Kohsaka, D. H. Lee, M. Azuma, M. Takano, H. Takagi, and J. C. Davis, Nature (London) **430**, 1001 (2004).
[87] S. A. Kivelsom, I. P. Bindloss, E. Fradkin, V. Oganesyan, J. M. Tranquada, A. Kaptitulnik, and C. Howald, Rev. Mod. Phys. **75**, 1201 (2003).
[88] M. Vojta, T. Vojta, and R. K. Kaul, cond-mat/0510448 (unpublished).
[89] S. A. Kivelson, E. Fradkin, and V. J. Emery, Nature (London) **393**, 550 (1998).
[90] A. Sherman and M. Schreiber, Int. J. Mod. Phys. B **19**, 2145 (2005).
[91] G. Seibold and J. Lorenzana, cond-mat/0509175 (unpublished).
[92] C. Stock, W. J. L. Buyers, R. A. Cowley, P. S. Clegg, R. Coldea, C. D. Frost, R. Liang, D. Peets, D. Bonn, W. N. Hardy, and R. J. Birgeneau, Phys. Rev. B **71**, 024522 (2005).
[93] V. Hinkov, P. Bourges, S. Pailhes, Y. Sidis, A. Ivanov, C. T. Lin, D. P. Chen, and B. Keimer, cond-mat/0601048 (upublished).